Acta Geochim
https://doi.org/10.1007/s11631-026-00856-4

ORIGINAL ARTICLE

Baseline data on selenium micronutrient concentration in parts of Southern Nigeria show provenance and paleodepositional controls

Aitalokhai J. Edegbai[1,2] · Jennifer B. Owonaro[3] · Jubemi A. Pajiah[2] · Erepamo J. Omietimi[1,4] · Nils Lenhardt[1] · Justina E. Ukpebor[5]

Received: 1 August 2025 / Revised: 26 January 2026 / Accepted: 28 January 2026

Abstract This study evaluates the Se concentration and examines the geologic controls on Se concentration in Upper Cretaceous and Palaeogene mudrocks in parts of Southern Nigeria. Geochemical analysis [(major and trace elements, total organic and inorganic carbon (TOC and TIC)] and pH measurements were conducted on seventy-three mudrock outcrop samples from the estuarine Late Campanian to Mid-Maastrichtian Mamu Formation and ditch cuttings from water wells that penetrated the marine Palaeogene Imo Formation from the Anambra basin and Niger Delta basin in the Southern Benue Trough. Selenium concentration in the Palaeogene calcareous marine mudrock samples reaches up to 21 ppm, significantly exceeding data observed in the Upper Cretaceous estuarine mudrock samples. Covariation charts suggest that Se adsorption onto clay, Fe-minerals, and limited sorption by organic matter in the estuarine mudrock samples are compared to adsorption onto clays, calcite, and very limited sequestration by Fe-minerals observed in the calcareous marine mudrocks. Principal component analysis and redundancy analysis reveal a dominant influence of carbonate minerals on selenium sequestration. Additionally, the Palaeogene calcareous marine mudrock samples are less acidic (mean pH 5.92) than the Upper Cretaceous estuarine mudrocks with a mean pH of 5.02. Therefore, it is hypothesized that higher pH may slightly promote the bioavailability of Se, resulting in higher Se intake by plants in areas underlain by the Palaeogene calcareous mudrocks.

Keywords Hydrothermal influence; provenance · Inorganic carbon · Benin flank · Benue Trough

1 Introduction

Selenium (Se) is an important micronutrient that boosts antioxidant activity, immune and brain function, provides relief for HIV/AIDS sufferers, suppresses side effects of chemotherapy/radiotherapy, reproductive health, and so on. (Rayman 2000, 2020 Abulude et al. 2006; Yakubu et al. 2014) when imbibed optimally. The recommended adult daily Se intake by the WHO, essential for health, is 50–70 µg/day (Finley 2006; Sakr et al. 2018). Insufficient or excessive Se intake can have deleterious effects on humans and animals. Common diseases associated with long-term insufficient daily Se intake include congestive cardiomyopathy, necrosis, cancer, hyperthyroidism, Graves' disease, various nutritional diseases, among others (Salonen et al. 1982). Additionally, people suffering from atrophic diseases such as arthritis and cirrhosis commonly suffer from insufficient Se intake (Eroglu et al. 2012). Similarly, long-term excessive daily Se intake is associated with dermatological, gastrointestinal, and nervous system

Supplementary Information The online version contains supplementary material available at https://doi.org/10.1007/s11631-026-00856-4.

✉ Aitalokhai J. Edegbai
u24120074@tuks.co.za

1 Department of Geology, University of Pretoria, Private Bag X20, Pretoria 0028, South Africa

2 Department of Geology, University of Benin, Benin City, Nigeria

3 Department of Marine Geology, Nigeria Maritime University, Okerenkoko, Warri South, , Delta State, Nigeria

4 Department of Geology, Niger Delta University, Amassoma, Nigeria

5 Department of Chemistry, University of Benin, Benin, Nigeria

Published online: 03 March 2026

disorders, diabetes, memory loss, fatigue, cancer, paralysis, and death (Fordyce 2012).

Human dietary intake of Se comes from plants (cereals, grains, and vegetables), animal products (meat, milk, fish, and eggs), and water (Fairweather-Tait and Hurs 2010; Fordyce 2012; Dhillon and Dhillon 2015). Additionally, the Se concentration varies with food type. For example, the Se concentration is higher in egg yolk than in egg white (Latshaw and Osman 1975). Likewise, fish possess higher Se content than meat (Kieliszek et al. 2022). Similarly, higher Se concentrations have been reported in garlic, cereals, nuts, and mustard vegetables than in legumes (Kieliszek et al. 2022). Overall, seafoods supply the highest human dietary Se content (Dinh et al. 2018). Abulude et al. (2006) examined basic food items in Akure, SW Nigeria, and reported high concentrations of Se in millet, rice, tilapia, crayfish, milk, nuts, beans, and yams. Gbadebo et al. (2010) postulated a positive correlation between yam consumption and Se intake in Abeokuta, SW Nigeria.

Globally, about two billion individuals are deficient in Se, with developing countries (especially countries in sub-Saharan Africa) accounting for a large proportion of this number (Wang and Gao 2001; Wang et al. 2021; Gashu et al. 2021). For children under 2 years, breast milk is an important source of dietary Se. Ejezie et al. (2012) reported high levels of Se in colostrum (up to 75 µg/L) in comparison to other breast milk in Enugu, SE Nigeria. Ezeama et al. (2022) reported Se deficiency in breast milk among a significant number of lactating women in Awka, SE Nigeria, which underscores the need for maternal nutrition in improving the dietary Se intake of nursing mothers and in toddlers (Nwagha et al. 2011). There are also indicators that staple food crops exhibit varying Se concentrations due to geological and environmental factors. For example, Courtman et al. (2012) reported varying Se concentrations in maize crops in parts of South Africa due to constraints such as background soil concentrations and pH levels. Gashu et al. (2021) also arrived at similar conclusions using data from Malawi and Ethiopia. Similarly, there are reports of geospatial variability in blood Se concentration compiled from several African countries such as: Nigeria, Algeria, South Africa, Malawi, Democratic Republic of Congo, Ghana, Senegal, Kenya, Zambia, Egypt, Mozambique, Niger, Rwanda, Sudan, Uganda, Côte d'Ivoire, Ethiopia, Morocco, and Tanzania, which is a consequence of dietary Se intake underpinned by geologic and environmental factors (Ligowe et al. 2020). In the Middle East, insufficient dietary intake of Se has also been reported (Kieliszek et al. 2022). In the developed world and in parts of Africa, measures such as the introduction of Se fertilizer, livestock supplements, (Se) biofortified plants, among others, have been introduced to boost dietary Se intake in plants, animals, and ultimately humans (Lyons et al. 2003; Fisinin et al. 2009; Winkel et al. 2012).

The nature of the underlying geology primarily determines Se concentration in soils and water (Xu et al. 2024). Therefore, the mobility of Se from rocks/soil into water, plants, and animals globally is constrained by the background Se concentration, alongside the pH, Eh, and grain size (Frankenberger and Benson 1994; Fordyce et al. 2010; Wang and Gao 2001; Dhillon and Dhillon 2014). Selenium concentration is variable in the different classes of rocks. Excluding volcanic rocks with mantle-derived magma and igneous rocks hosting sulphide deposits, some of the lowest Se concentrations are recorded in most igneous rocks (Fordyce, 2012; Fordyce et al. 2010). Also worthy of note is that the Se concentration decreases with an increase in metamorphism (Malisa 2001). On the other hand, sediments/sedimentary rocks, especially clay-rich mudrocks with high organic richness and coal, typically show high Se levels (Koljonen 1973; Poole et al. 1979; Adriano 2001). The reason adduced for the higher Se concentration observed in organic-rich mudrocks is the high capacity of clay minerals and organic matter to sequester Se from water (Measures and Burton 1980).

Selenium-rich soils have been reported in the United States, China, Australia, India, Ireland, South Africa, and Israel (Favorito et al. 2017; Zheng et al. 2022; Eiche et al. 2015). In Nigeria, the very few studies on baseline Se concentrations in soils and rocks are mostly lacking adequate geologic context and stratigraphic control (Aremu et al. 2010; Kolawole and Obueh 2013; Nganje et al. 2020). An average of 1.13 mg/kg has been reported in Nasarawa (Aremu et al. 2010), a state in the North Central region of Nigeria. In the Cross River and Akwa Ibom States, in southern Nigeria, the Se content varies from 0.002 to 8.08 mg/kg (Kolawole and Obueh 2013).

Most Se-centered studies in developing countries such as Nigeria have focused on Se concentration in food and human body fluids (Gbadebo et al. 2010; Nwagha et al. 2011; Ejezie et al. 2012; Ezeama et al. 2022). However, baseline data on Se concentration constrained by geologic and stratigraphic components, needed to predict and identify Se-deficient/enriched areas, are lacking. Specifically, this research aims to evaluate the background Se concentration in Upper Cretaceous and Palaeogene mudrocks as well as provide insight into the geologic controls on the concentration of selenium.

2 Tectonics and stratigraphy

2.1 Maastrichtian to Palaeocene tectonostratigraphy of the southern Benue Trough

The Benue Trough (Fig. 1a) is a paleotectonic structure that was formed during the last stages of the breakup of Gondwana (Lenhardt et al. 2025). This strike-slip influenced rift

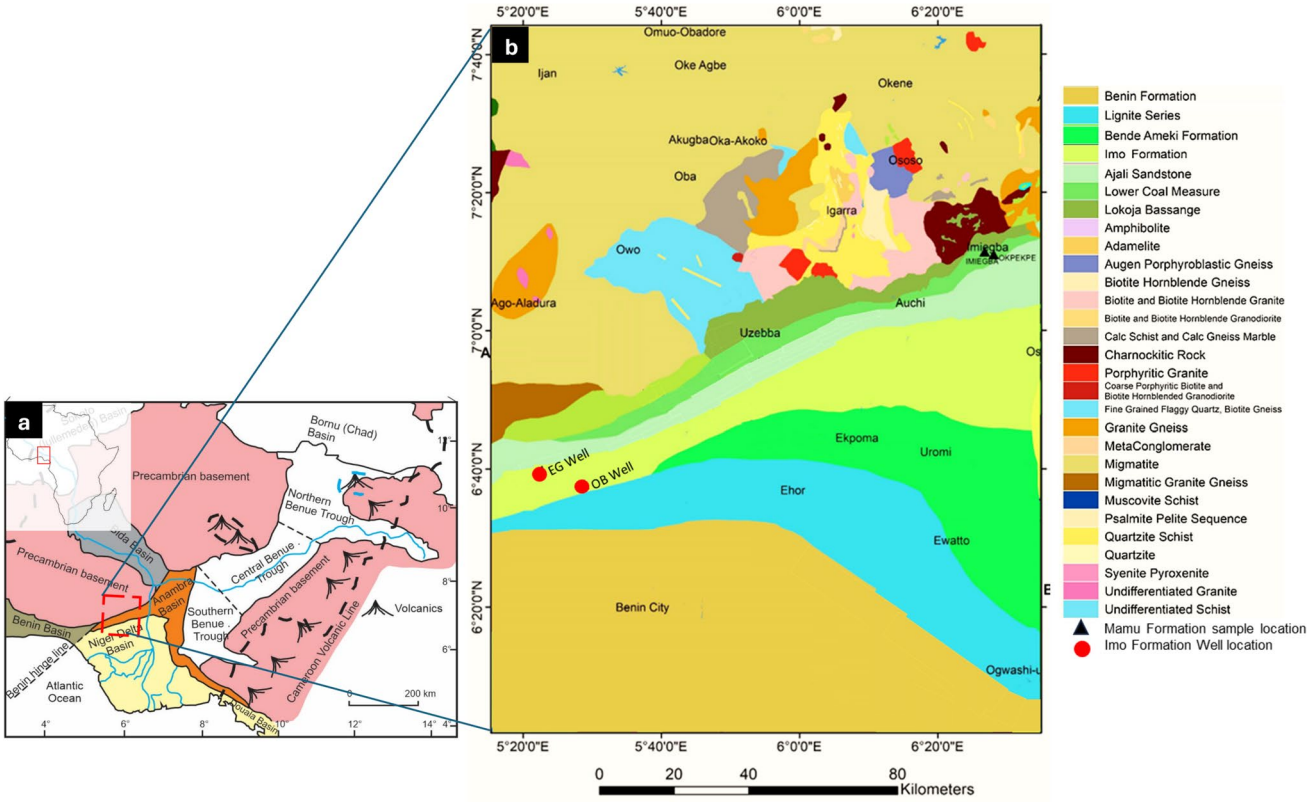

Fig. 1 **a** Map of Nigeria showing its sedimentary basins. The red box depicts the study area; **b** Geological map showing the locations of the EG and OB wells (Imo Formation), together with the Imiegba and Okpekpe outcrop locations (Mamu Formation) (Adapted from Edegbai et al. 2019; NGSA, 2022)

basin trends NE-SW over an area of circa 100,000 km^2, with a basin fill of up to 6000 m (Ofoegbu 1984; Benkhelil 1989; Gebhardt et al. 2020; Lenhardt et al. 2025). The Benue Trough has three arbitrarily subdivisions—the Northern, Central, and Southern Benue Trough (Fig. 1a) (Nwajide 2013). The southern Benue Trough is the deepest trough segment with a multicycle tectonic history comprising: (1) Barremian to Coniacian crustal extension evidenced by a rift and post-rift sag phase (and associated magmatism/hydrothermal mineralization); (2) Santonian crustal shortening evidenced by inversion (and associated sediment uplift and erosion, folding, faulting, and perhaps magmatism); (3) Campanian to Recent post-inversion crustal extension evinced by a sag to passive margin phase (Lenhardt et al. 2025). The post-inversion crustal extension represents the last active phase in the (Southern) Benue Trough's tectonic history, which was first characterised by tectonic subsidence of the Anambra Basin west and east of the Abakaliki anticlinorium.

Sedimentation within the post-Santonian depocenters was typified in stratigraphic order by the Nkporo Group, Mamu Formation, Ajali Formation, and Nsukka Formation (Nwajide 2013). The foregoing lithostratigraphic units were blanketed by mudrock, subordinate limestone, and sand of the Imo Formation (coeval with the subcropping Akata Formation) deposited during widespread flooding of the South Atlantic Ocean, which began in the Selandian-Thanetian Age (Fig. 2) (Short and Stauble 1967; Reijers et al. 1996; Nwajide 2013). This marked the onset of deposition in a passive margin setting of what is now known as the Niger Delta Basin. Subsequent post-Thanetian relative sea level fall promoted the active development of regressive deltaic deposits typified by the Ameki Group-Ogwashi Asaba Formation (coeval with the subcropping Agbada Formation) and the Benin Formation, which are paralic and continental deposits respectively (Avbovbo 1978).

2.2 Lithostratigraphy of the Mamu and Imo formations

2.2.1 The Imo Formation

The Palaeogene Imo Formation (Figs. 1, 2 and 3) is comprised primarily of grey calcareous fossiliferous mudrock;

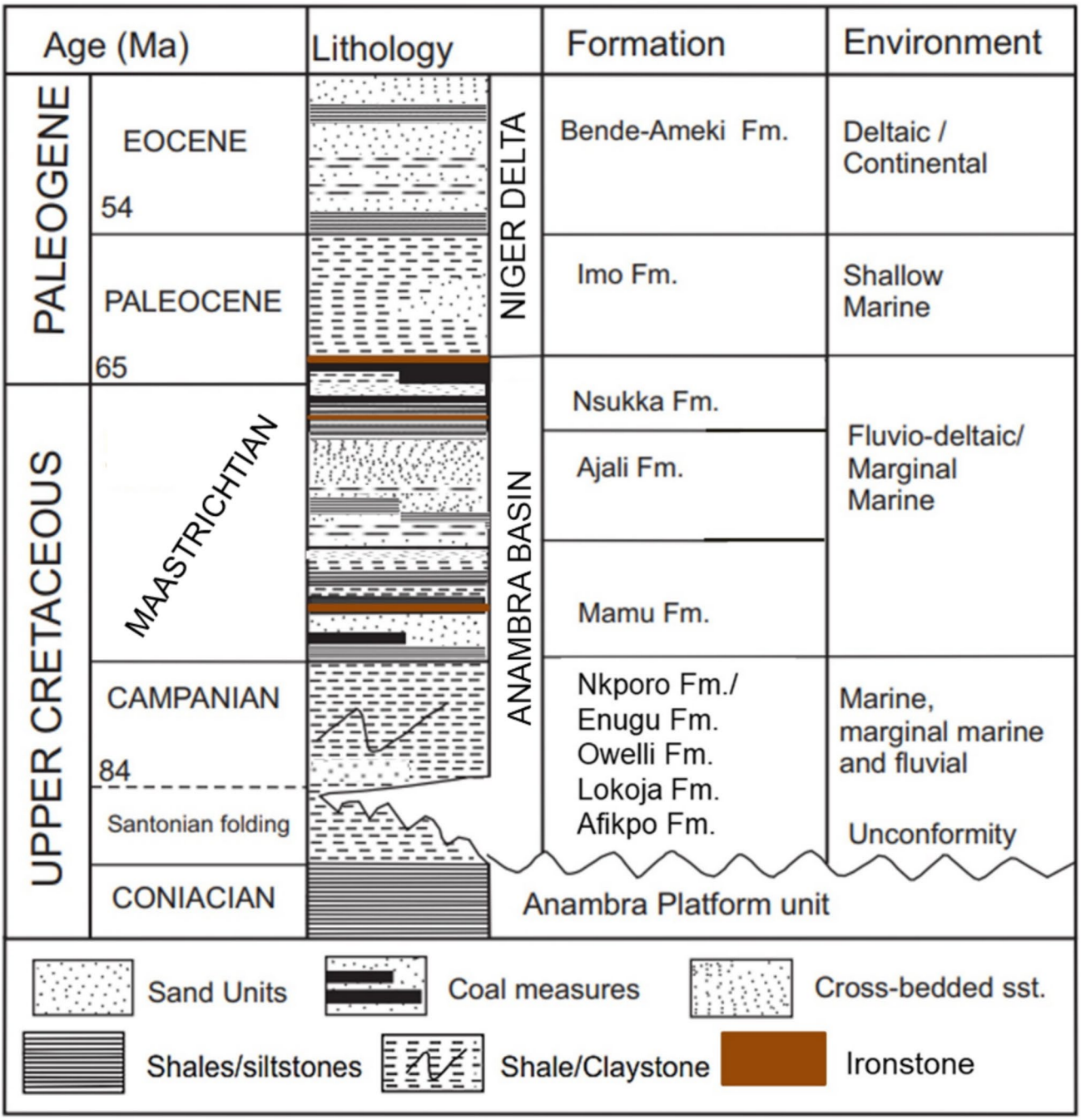

Fig. 2 Post-Santonian lithostratigraphy of Southern Benue Trough, Nigeria (modified from Tijani et al. 2010)

hence, the name Imo Shale is common in older manuscripts (Ekwenye et al. 2014). Limestone, ironstone, and sand units are occasionally interstratified with this grey calcareous fossiliferous mudrock. The thickness of this lithostratigraphic unit varies from < 100 m in the western fringe of the Niger-Delta Basin (study location) to over 1000 m in the central part of the basin (from well data). Data from Jimoh et al. (2024) indicate detrital materials were sourced from a felsic to intermediate provenance under prevailing warm, humid paleoclimatic conditions.

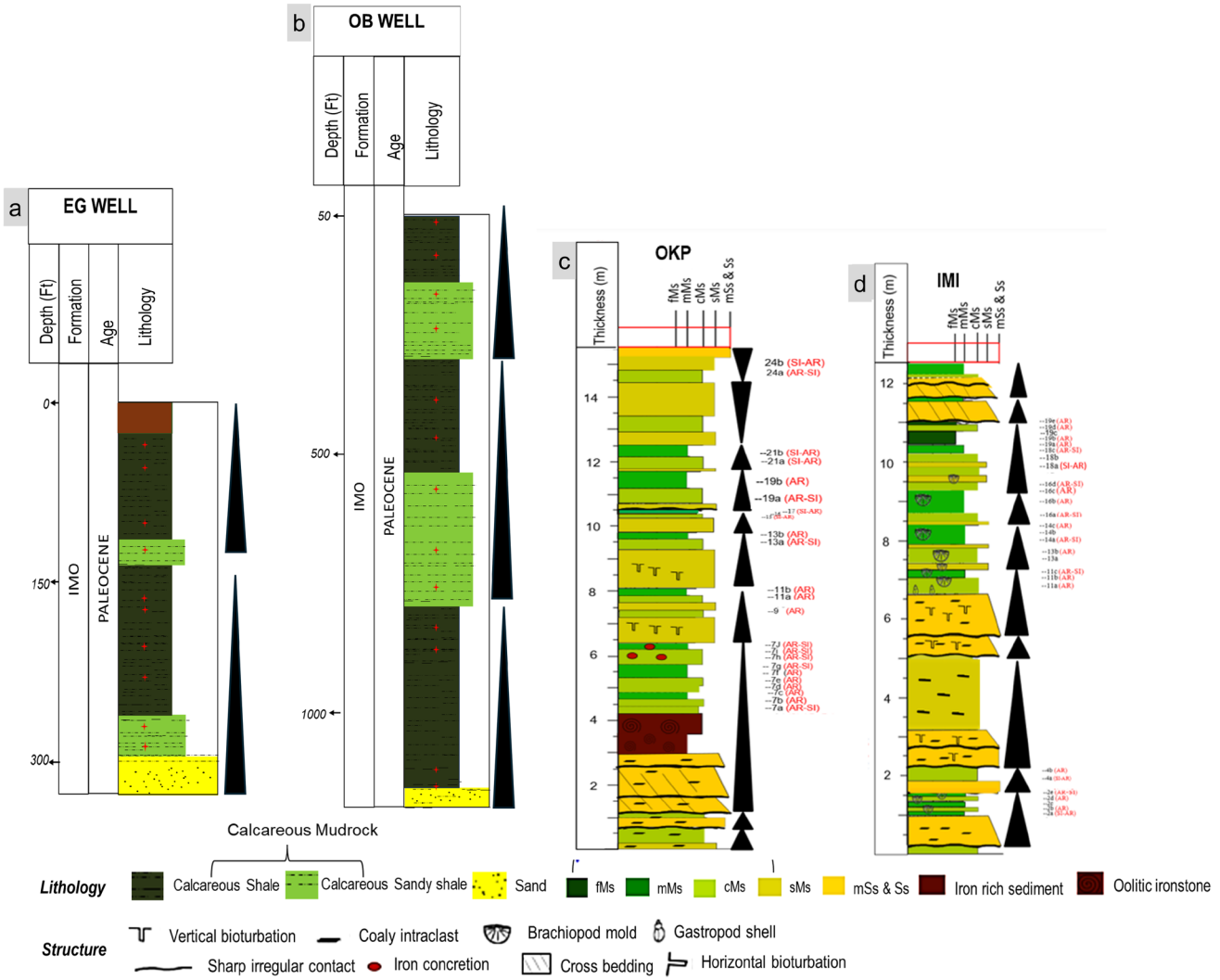

Fig. 3 **a**,**b**. Lithologic sections of the OKP and IMI locations (adapted from Edegbai et al. 2019); **c**,**d**. lithologic sections of the EG and OB wells

2.2.2 *The Mamu Formation*

The Mamu Formation (Figs. 1, 2 and 3) spans an age range from Latest Campanian to Mid-Maastrichtian along an N-S transect (Zaborski 1983; Gebhardt 1998). In addition, this lithostratigraphic unit consists of several lithologic units with thicknesses varying from less than 20 m in basin flanks to > 600 m in the subsurface (Ladipo 1988; Gebhardt 1998; Nwajide 2013; Edegbai et al. 2019). In the study area, the Mamu Formation is characterised by lithologic units such as dark and light-coloured mudrocks, heterolithics, sandstone, ironstone, and coal (Edegbai et al. 2019). Limestone units have also been reported elsewhere (Gebhardt 1998; Akande and Mücke 1993).

Palaeoenvironmental reconstruction has revealed depositional conditions varying from estuarine paleoenvironment in the flanks to shallow marine in the basin center and southwards (Okoro and Igwe, 2018; Dim et al. 2019; Edegbai et al. 2019). Provenance and paleoclimate studies revealed a felsic to intermediate provenance comprised of pre-Santonian sedimentary strata and Precambrian igneous and metamorphic detritus that was provided under prevailing warm and humid paleoclimatic conditions (Edegbai et al. 2019).

3 Methodology

3.1 Lithological analysis and sampling

Comprehensive description and logging, involving visual textural analysis complemented by dilute HCl treatment of hand specimens, formed the basis for identifying lithological changes across outcrops and subcrops (cuttings) in the studied area (Lazar et al. 2015). These preceded the selection of mudrock samples for geochemical and pH analyses.

3.1.1 Sampling

Since organic-rich mudrocks and coal commonly possess higher selenium concentrations than sandstone units, sampling was restricted to mudrock intervals. Seventy-three mudrock samples were randomly obtained from measured sections of the Mamu Formation at exposed road cuts at Imiegba (IMI) and Okpekpe (OKP), Benin flank, SW Anambra Basin (Figs. 1b, 3a-b). For the Imo Formation, 23 mudrock samples were randomly collected from ditch cuttings of the EG and OB, water wells near Benin City, Northern Delta depobelt, and Niger-Delta Basin (Figs. 1, 3c-d).

3.2 Major and trace elements analysis

The analytical protocol employed for the geochemical analysis of Mamu Formation samples involved X-ray fluorescence (XRF) and inductively coupled plasma mass spectrometry (ICP-MS) for major and trace elements, respectively, at the Bureau Veritas Mineral Laboratories, Vancouver, Canada. This analysis was conducted in 2016. Sample preparation for XRF analysis entailed milling and homogenising 5 g of representative sample material, which was then dehydrated in an oven at 105 °C. The oven-dried samples were roasted and fused into glass beads in platinum-gold crucibles with a lithium tetraborate flux. The fused beads were then analyzed using PANalytical Axios Max XRF equipment. The sample preparation protocol for the ICP-MS analysis entailed near-total digestion of 0.25 g of milled material using a mix of mineral acids consisting of $2H_2O$: 2HF: $HClO_4$: HNO_3. The solution was subsequently mixed with HCl (50% v/v) in a hot block, heated up, and allowed to cool. The resulting solution was raised to volume using dilute HCl and thereafter analysed by PerkinElmer ELAN 9000 ICP-MS. As a precautionary measure, duplicates of samples, standards (OREAS 25A-4A, OREAS 45E, GBAP-3, NIST 600, NIST698 and ROCK-VAN), and blanks were run at regular intervals, with over 95% accuracy. The minimum detection limits (MDL) for trace elements varied from 1 ppm in Se and zinc (Zn) to 0.1 ppm in others. The MDL for Se was similarly, i.e., MDL for major elements varied from 0.001% in sodium and titanium (Na and Ti) to 0.01% in others. The Se concentration recorded in the standards varied from 1 to 5 ppm.

The geochemical analysis of the Imo Formation was conducted in 2023 using sodium peroxide fusion with ICP-MS measurement at Activation Lab, Ancaster, Ontario, Canada. The experimental procedure involved mixing milled Imo Formation samples with sodium peroxide flux (in a 1:6 ratio) and heating in a zirconium crucible. The samples were then acidified with concentrated HNO_3 and HCl and were measured using ICP-MS. To ensure data accuracy, duplicates of samples, standards (CZN-4), and blanks were run at regular intervals with over 95% accuracy. The minimum detection limits (MDL) for trace elements varied from 30 ppm in chromium (Cr), through 8 ppm in Se, to 0.1 ppm uranium (U) in others. Similarly, MDL for major elements varied from 0.001% in Sodium and Titanium (Na and Ti) to 0.01% in others. The Se concentration reported in the standard varied from 86.7 to 93 ppm in the standards, while the blank samples were below the detection limit of 8 ppm. The authors are assuming that the differences in analytical protocols and laboratory conditions do not adversely impact data quality. Enrichment factors (EF) of certain trace elements were calculated as:

$$X^{\mathrm{EF}} = (X/\mathrm{Al})_{\mathrm{sample}}/(X/\mathrm{Al})_{\mathrm{WSA}}$$

where X and Al represent concentrations of elements X and Al in weight percent, respectively. The observed data from the samples were normalized using the world shale average shale (WSA; Wedepohl 1971, 1991).

3.3 Bulk geochemical analysis

The total carbon (TC), total inorganic carbon (TIC), and total organic carbon (TOC) measurements were undertaken at the Stable Isotope Mass Spectroscopy Laboratory, Department of Geological Sciences, University of Florida, US. The experimental procedure for TC measurement entailed weighing 50 mg of milled samples into tin capsules, which were subsequently loaded into a Carlo Erba NA1500 CNHS analyser. The TIC experimental procedure involved weighing 15 mg of milled samples into vials in a CO_2 coulometer (UIC 5014) coupled to an automated carbonate preparation (AutoMate) device to measure, wherein free oxygen in the samples was well expelled before treatment with HCl and heating. The CO_2 expelled was trapped and computed as the TIC present in each sample. TOC was subsequently calculated by subtracting TIC from TC.

3.4 Measurement of pH

Ten grams (10 g) of selected milled samples were loaded into beakers and mixed with 40 ml of de-ionised water. The mixture was stirred with a glass rod and allowed to settle for 2 min. The pH of the sample was subsequently measured using a Hannah instrument HI 2210 pH meter in the Geochemistry Laboratory, Department of Geology, University of Benin, Nigeria. For data accuracy and reproducibility, the pH meter was calibrated with in- house standards after repeat measurements.

3.5 Statistical treatment of data

Pearson correlation coefficients were calculated with two-tailed significance tests and 95% confidence intervals estimated using Fisher's z transformation; *p* values were adjusted for multiple testing using the Benjamini–Hochberg false discovery rate procedure.

Sensitivity testing was conducted using a robust median absolute deviation (MAD) criterion to identify and exclude potential outliers. This analysis yielded consistent correlation magnitudes, overlapping confidence intervals, and identical significance patterns, indicating that the observed selenium–geochemical relationships are not driven by a small number of extreme observations.

In addition, unconstrained and constrained multivariate analyses were applied to treat the combined dataset to separate co-varying geochemical controls on selenium. Analyses were performed on $\log_{10}$-transformed and standardized concentrations and restricted to samples with complete data across all variables ($n = 34$), ensuring consistency with the robust statistical framework used in the correlation analysis. Principal component analysis (PCA) was used to identify the dominant axes of natural covariance among selenium, carbonate indicators (Ca, Mg, Sr, TIC, %calcite), siliciclastic/provenance proxies (Al, Si, Ti, Th), redox-sensitive metals (Fe, Zn, Ni, Co, V, Cr), and total organic carbon (TOC). To explicitly test and quantify these controls, redundancy analysis (RDA) was conducted using carbonate, provenance, redox, and organic matter proxies as explanatory variables.

4 Results

The results of the elemental analyses and pH measurements are detailed in Table 1.

4.1 Lithology

The cuttings from the OB and EG wells (Imo Formation, Fig. 3a-b) show a succession of calcareous sandstone, calcareous sandy shale, and calcareous shale, all of which liberate CO_2 when tested with dilute HCl. The calcareous sandy shale and calcareous shale are collectively referred to as calcareous mudrocks. The IMI and OKP outcrops (Mamu Formation; Fig. 3c-d) exhibit a succession of lithologic units, interpreted as dark grey and cream-colored mudrocks, sandstone, and oolitic ironstone (Edegbai et al. 2019).

4.2 Major elements (Si, Ca, Fe, K, Mg, Ti, and Al)

4.2.1 Imo Formation

The mean values of the major elements (ME) from the calcareous marine mudrocks are 20.06 wt%, 0.83 wt%, 7.05 wt%, 0.47 wt%, 5.50 wt%, 2.03 wt%, 6.24 wt% for Si, K, Al, Ti, Fe, Mg, and Ca, respectively (Fig. 4a). Excluding Fe, Ca, Mg, and Ti, the concentrations of Si, K, and Al, recorded from the Imo Formation calcareous mudrock samples, fell below the respective World Shale Average concentrations [(WSA = 27.53 wt.% for Si, 2.99 wt.% for K, 8.84 wt% for Al, 0.47 wt% for Ti, 5.36 wt% for Fe, and 1.57 wt% for Ca and Mg, respectively (Wedepohl 1971, 1991)] (Fig. 4a). Additionally, the concentrations of the ME show variability along the well bore, with the greatest ME variability observed in the EG well. For the OB well, the Si concentration is higher in the bottom samples, while greater concentrations of Fe, Mg, Al, K, and Ti were recorded in the midsection (Fig. 3a-b). In general, the Imo Formation calcareous mudrocks possess higher Fe, Mg, K, and Ca concentrations than the Mamu Formation dark mudrock samples, which show higher Si, Al, and Ti concentrations (Fig. 4a).

4.2.2 Mamu Formation

The mean ME concentration recorded from the Mamu Formation dark mudrock samples is 24.80 wt%, 0.76 wt%, 12.25 wt%, 0.75 wt%, 2.94 wt%, 0.18 wt%, and 0.07 wt% for Si, K, Al, Ti, Fe, Mg, and Ca, respectively (Fig. 4a). Except for Ti and Al, the mean concentrations of Si, Fe, Mg, K, and Ca, recorded from the dark mudrock samples, are below the respective WSA (Fig. 4a). In the IMI location the samples close to the top section show higher ME concentrations when compared to samples from the bottom and top section (Fig. 3b). Conversely, in the OKP location, the dark mudrock samples at the bottom and mid-sections show higher Al, Fe, Ca, and Mg. In addition, a gradual increase of Si and Ti concentrations is observed towards the top section (Fig. 3a). Overall, the OKP section shows greater variability in the concentration of Si, K, Al, Fe, and Mg.

Table 1 Geochemical and pH data of the Mamu Formation (IMI and OKP locations) and Imo Formation (OB and EG wells)

Depth (m)	Mamu	Fe	Ca	Al	Mg	K	Si	Ti	TiO_2	Mn	Ni	Co	U	Mo	V	Cu	Cr	Se	Ba
1.26	IM 2B	2.68	0.04	12.86	0.22	0.99	23.00	0.86	1.44	0.0055	42.7	23	6.8	1.8	159	25.9	103	1	158
1.41	1 M 2C	2.55	0.03	12.41	0.23	1.00	24.82	0.97	1.62	0.0059	32.9	13.2	7.2	1.5	161	19.6	105	-	165
1.56	1 M 2D	2.7	0.03	11.49	0.24	1.01	25.20	0.87	1.45	0.0056	32.1	16.1	7	0.6	150	28.7	99	2	152
1.71	1 M 2E	4.29	0.06	11.87	0.30	0.98	23.65	0.84	1.40	0.0158	46.7	22.5	5.9	1.3	151	22.7	109	-	147
2.08	IM 4A	4.23	0.02	9.9	0.17	0.71	26.83	0.71	1.18	0.0065	23.5	12	5.4	1	123	14.7	75	1	106
6.89	IM 11A	6.92	0.07	12.61	0.22	0.60	22.81	0.66	1.10	0.0082	53.5	30.7	9.8	1	139	30.5	95	2	104
7.09	IM 11B	3.95	0.05	15.81	0.29	1.00	20.71	0.69	1.15	0.0095	50.3	21	7	1	144	32.1	114	2	141
7.29	IM 11C	4.73	0.19	11.85	0.34	1.14	25.01	0.66	1.11	0.0144	54.7	31.2	8.5	0.6	203	28.1	125	–	180
7.62	IM 13A	7.08	0.12	12.86	0.41	1.00	21.78	0.60	1.01	0.0917	58.8	32	6.4	1.2	133	31.1	131	–	130
7.82	1 M 13B	3.27	0.04	14.18	0.30	1.06	22.58	0.76	1.26	0.0077	47.7	22.5	6	1.1	146	35.1	113	3	164
8.03	IM 14A	4.99	0.48	11.56	0.32	1.08	23.75	0.64	1.07	0.021	61.9	29.9	8.3	2	131	32.2	111	1	115
8.73	IM 16A	12.52	0.25	11.54	0.42	1.20	18.51	0.39	0.65	0.2527	59.1	26.1	4.5	2.2	104	28.9	104	2	106
8.98	IM 16B	6.54	0.17	12.08	0.41	1.36	20.66	0.46	0.77	0.084	60.9	25.1	4.7	1.7	103	24.3	99	2	136
9.23	1 M 16C	3.78	0.08	12.58	0.35	1.45	22.44	0.54	0.90	0.0212	46.1	15.1	4.4	1.5	118	19.2	101	–	155
9.48	1 M 16D	2.82	0.06	11.73	0.30	1.34	25.10	0.57	0.95	0.0076	39.2	19.2	4.8	0.5	115	17.9	97	2	176
9.87	IM 18a	0.85	0.575	9.18	0.13	1.06	28.85	0.41	0.68	0.003637643	49.1	3.7	11.4	0.9	67	10.5	68	2	653
10.33	IM 18C	1.34	0.1	16	0.17	0.81	22.30	0.66	1.10	0.0041	32.9	6.3	10.8	1.5	94	24.2	94	3	225
10.5	IM 19A	1.85	0.09	15.19	0.24	1.10	22.48	0.61	1.01	0.0037	28.2	7.6	8.6	2	111	36.5	107		257
10.64	IM 19B	2.34	0.06	15.62	0.24	1.10	21.78	0.57	0.96	0.0032	43.2	13.4	7.5	1	109	43.1	100	2	235
10.92	IM 19D	3.19	0.05	14.52	0.19	0.92	21.03	0.61	1.02	0.0066	54.5	36.8	5.6	1	102	209.1	105	1	176
11.06	IM 19E	1.81	0.04	15.79	0.22	1.05	22.86	0.71	1.18	0.0048	26.9	7.4	5.9	1.9	128	19.3	109	2	202
1.11	IM 2A	3.04	0.03	11.87	0.16	0.74	24.03	0.76	1.26	0.0041	29.2	9.5	6	1.7	131	11.3	101	2	186
2.24	IM 4B	4.27	0.01	7.23	0.11	0.48	29.22	0.27	0.45	0.006815248	7.6	2.1	3.4	2.3	27	6.4	27	1	41
8.23	IM 14B	2.82	0.06	11.73	0.28	1.29	25.10	0.57	0.95		39.2	19.2	4.8	0.5	115	17.9	97	2	176
8.43	IM 14C	6.09	0.21	12.61	0.39	1.15	20.75	0.52	0.87	0.0202	75.4	27.5	7.7	3.3	110	44	99	2	96
10.13	IM 18B	1.35	0.09	11.04	0.14	0.70	22.78	0.61	1.02	0.004027192	54.5	36.8	5.6	1	102	209.1	105	1	176
	Mean	3.92	0.11	12.63	0.26	1.01	23.30	0.63	1.06	0.004	44.94	20.17	6.73	1.39	121.26	43.33	100.04	1.81	175.00
	SD	2.40	0.13	2.12	0.09	0.23	2.45	0.15	0.26	0.02	14.96	10.37	1.96	0.64	32.92	54.02	19.12	0.60	105.89
4.28	OK 7A	3.3	0.02	10.93	0.12	0.46	25.24	0.86	1.44	0.0039	33.8	16.2	7.2	3.2	95	18.3	92	–	118
4.5	OK 7B	2.77	0.02	6.69	0.06	0.23	33.84	0.63	1.05	0.0081	21.6	7.8	5.6	6.4	69	13	118	–	86
4.72	OK 7C	6.23	0.03	14.21	0.11	0.46	17.81	0.50	0.83	0.0178	65.7	36.9	9	7.9	114	40.7	102	3	78
4.94	OK 7D	4.96	0.02	14.63	0.10	0.42	18.98	0.60	1.00	0.0047	57.1	28.8	11.6	2.9	93	38.8	104	3	96
5.16	OK 7E	2.36	0.03	13.62	0.08	0.40	21.97	0.94	1.56	0.0022	43.9	22.9	8.7	2.5	101	25.7	91	2	147
5.38	OK 7F	1.93	0.02	14.2	0.08	0.42	21.13	0.72	1.21	0.0051	88.4	29.1	8.5	1.5	98	26.7	72	2	115
5.6	OK 7G	1.84	0.03	10.1	0.07	0.46	27.21	0.73	1.22	0.0033	52.5	12.5	7.9	1.8	105	18	70	2	144
5.82	OK 7H	1.2	0.01	10.5	0.07	0.37	27.72	0.83	1.38	0.0049	26.4	6.2	8.2	2.6	67	15.7	97	2	111

Table 1 (continued)

Depth (m)	Mamu	Fe	Ca	Al	Mg	K	Si	Ti	TiO_2	Mn	Ni	Co	U	Mo	V	Cu	Cr	Se	Ba
6.04	OK 7I	1.38	0.02	13.47	0.07	0.39	24.77	0.87	1.45	0.0026	26.9	8.9	12	2.8	83	30	86	2	120
6.28	OK 7 J	1.59	0.02	11.99	0.07	0.44	26.74	1.03	1.71	0.0046	29.4	6.2	13.7	4.3	104	29.9	119	1	151
7.25	OK 9	0.79	0.03	14.32	0.08	0.42	24.35	0.76	1.27	0.002	47.2	6	10.8	1	88	19.1	88	–	126
7.74	OK 11A	1.73	0.01	13.49	0.11	0.64	25.34	0.99	1.66	0.0054	25.3	5.6	10.3	3.3	103	17.8	105	–	223
7.94	OK 11B	1.55	0.03	13.31	0.16	0.88	24.68	1.05	1.75	0.0027	22.2	5	8	2.1	110	13.8	93	–	193
9.36	OK 13A	1.25	0.01	11.54	0.07	0.45	28.47	0.88	1.46	0.0038	25.4	5.2	10.5	3.5	86	27.1	99	2	151
9.63	OK 13B	1.11	0.02	12.99	0.08	0.50	24.96	0.99	1.65	0.003	29.2	6.6	14	1.8	96	29.9	94	–	156
10.3	OK 15	0.63	0.02	7.48	0.05	0.51	34.87	0.94	1.56	0.0037	27.3	3.1	8.3	1.5	54	13.7	56	1	193
10.5	OK 17	0.72	0.02	10.23	0.05	0.46	30.20	0.90	1.50	0.0046	42.7	4.6	11.8	1.8	61	36.7	84	–	177
10.8	OK 19A	0.64	0.02	12.03	0.06	0.41	27.25	0.93	1.55	0.0026	29.8	6.1	19.5	1.1	76	59.3	96	1	154
11.3	OK 19B	1.05	0.01	13.66	0.08	0.46	25.20	1.04	1.74	0.0026	35.3	6.5	12.1	1.9	88	32.7	100	–	185
11.95	OK 21A	1.19	0.03	9.64	0.09	0.60	31.46	1.14	1.90	0.0027	24.1	3.3	12.4	1	94	20.3	72	3	253
12.33	OK 21B	1.6	0.02	10.67	0.10	0.62	29.40	1.11	1.85	0.0034	22.3	4.2	10.8	1.7	97	17.8	90	2	246
14.62	OK 24A	0.63	0.01	12.67	0.06	0.42	26.83	0.96	1.59	0.0021	33.9	5.3	31.2	1.5	76	63.6	86	–	166
15.01	0 k 24B	0.65	<0.01	8.96	0.05	0.41	32.63	0.88	1.47	0.004	25.9	4.2	11.5	1.9	73	26.4	76	–	146
	Mean	1.79	0.02	11.80	0.08	0.47	26.57	0.88	1.47	0.0043	36.36	10.49	11.46	2.61	88.30	27.61	90.87	2.00	153.70
	SD	1.40	0.01	2.23	0.03	0.12	4.34	0.16	0.27	0.0032	16.54	9.57	5.18	1.68	16.07	13.42	14.99	0.71	46.86
Mamu Av		2.94	0.07	12.25	0.18	0.76	24.80	0.75	1.25	0.01	40.99	15.72	8.91	1.95	106.10	36.10	95.82	1.88	165.20
63	OB 1	6.90	1.93	8.58	0.78	1.20	22.70	0.71	1.18	0.0541	80.00	15.70	2.30	3.00	88.00	45.00	130.00	15.00	368.00
125	OB 2	6.10	6.63	8.27	1.06	0.70	19.10	0.63	1.05	0.0514	70.00	18.30	4.20	4.00	140.00	49.00	140.00	15.00	136.00
195	OB 3	7.63	6.66	7.75	1.18	0.70	18.00	0.55	0.92	0.0505	100.00	21.40	6.30	7.00	133.00	67.00	130.00	13.00	108.00
265	OB 4	4.97	6.41	7.32	2.01	0.70	19.80	0.51	0.85	0.0849	90.00	17.80	4.20	5.00	149.00	64.00	160.00	9.00	97.00
395	OB 5	5.43	3.66	8.72	1.84	0.90	21.00	0.57	0.95	0.0531	70.00	18.90	3.00	6.00	160.00	51.00	200.00	13.00	100.00
465	OB 6	5.12	2.26	9.62	1.52	0.90	21.90	0.58	0.97	0.0371	60.00	19.60	3.00	4.00	164.00	43.00	150.00	16.00	114.00
565	OB 7	4.45	7.04	7.32	2.07	0.70	20.10	0.47	0.78	0.0604	50.00	16.00	2.30	4.00	132.00	27.00	130.00	16.00	98.00
675	OB 8	5.15	5.71	7.56	2.07	0.80	20.30	0.48	0.80	0.0817	60.00	17.90	3.60	5.00	138.00	33.00	160.00	14.00	110.00
745	OB 9	4.48	5.49	7.89	2.75	0.90	19.80	0.46	0.77	0.0727	70.00	15.90	2.70	4.00	136.00	84.00	140.00	12.00	112.00
815	OB 10	5.13	3.22	9.41	1.94	1.20	21.60	0.57	0.95	0.0579	80.00	19.30	3.30	4.00	156.00	68.00	140.00	14.00	143.00
865	OB 11	5.51	4.54	8.46	1.94	1.10	20.90	0.51	0.85	0.0769	80.00	18.90	3.60	5.00	148.00	49.00	160.00	14.00	130.00
1085	OB 12	4.89	4.17	6.10	1.44	0.80	25.50	0.38	0.63	0.0604	70.00	16.50	3.00	4.00	107.00	53.00	100.00	13.00	86.00
1115	OB 13	4.83	4.53	8.10	2.02	0.90	21.40	0.51	0.85	0.055	140.00	22.50	4.40	4.00	130.00	69.00	130.00	12.00	115.00
	Mean	5.43	4.79	8.08	1.74	0.88	20.93	0.53	0.89	0.06	78.46	18.36	3.53	4.54	137.00	54.00	143.85	13.54	132.08
	SD	0.93	1.70	0.93	0.53	0.18	1.85	0.08	0.14	0.01	22.67	2.08	1.08	1.05	20.99	15.87	23.64	1.90	72.70
35	EG 1	3.83	1.49	5.57	1.84	0.70	30.00	0.55	0.92	0.0337	40.00	13.10	2.60	3.00	114.00	21.00	120.00	10.00	240.00
55	EG 2	3.77	9.68	5.41	4.19	0.70	16.20	0.31	0.52	0.102	50.00	11.90	2.00	4.00	99.00	27.00	120.00	9.00	370.00
100	EG 3	4.63	5.14	5.98	1.90	0.50	24.00	0.38	0.63	0.142	50.00	52.20	2.10	3.00	123.00	111.00	110.00	21.00	812.00

Table 1 (continued)

Depth (m)	Mamu	Fe	Ca	Al	Mg	K	Si	Ti	TiO_2	Mn	Ni	Co	U	Mo	V	Cu	Cr	Se	Ba
125	EG 4	6.53	15.60	2.54	3.51	0.30	10.70	0.18	0.30	0.293	50.00	17.10	3.90	6.00	68.00	19.00	70.00	14.00	2140.00
165	EG 5	4.33	4.27	5.55	2.58	0.70	25.50	0.42	0.70	0.0963	40.00	12.70	2.90	4.00	104.00	37.00	120.00	12.00	689.00
175	EG 6	5.43	5.46	7.94	2.12	1.00	19.10	0.47	0.78	0.0905	50.00	20.40	6.90	4.00	139.00	18.00	130.00	18.00	121.00
205	EG 7	5.75	3.21	8.27	2.02	1.40	20.90	0.54	0.90	0.106	50.00	19.20	4.30	5.00	152.00	23.00	140.00	11.00	134.00
235	EG 8	6.25	3.31	8.64	1.73	1.40	21.30	0.53	0.88	0.0743	50.00	19.40	3.40	6.00	157.00	42.00	150.00	12.00	138.00
275	EG 9	8.78	11.90	4.62	2.29	0.60	14.30	0.29	0.48	0.129	50.00	21.70	7.20	5.00	138.00	23.00	120.00	10.00	109.00
295	EG 10	6.55	21.10	2.47	1.83	0.40	7.35	0.15	0.25	0.0924	40.00	16.50	5.10	6.00	73.00	16.00	80.00	14.00	69.00
	Mean	5.59	8.12	5.70	2.40	0.77	18.94	0.38	0.64	0.12	47.00	20.42	4.04	4.60	116.70	33.70	116.00	13.10	482.20
	SD	1.54	6.35	2.16	0.82	0.38	6.93	0.15	0.24	0.07	4.83	11.67	1.86	1.17	30.96	28.41	24.59	3.81	636.94
Imo Fm. Av		5.50	6.24	7.05	2.03	0.83	20.06	0.47	0.78	0.09	64.78	19.26	3.75	4.57	128.17	45.17	131.74	13.35	284.30
WSA		5.36	1.57	8.84	1.57	2.99	27.53	0.47	0.784	0.085	68	19	0.47	1	130	45	90	0.6	580

Depth (m)	Mamu	Th	Th*10	Sr	Pb	Zn	Y	pH	TC	TIC	% calcite	TOC	Y/Ni	Cr/V	Fe/Ti	Al/(Fe + Al + Mn)	K/Al	Mg/Al
1.26	IM 2B	18.1	181	104	39.6	43	20.6	–	1.09	0.08	0.70	1.01	0.48	0.65	3.10	0.83	0.07	0.017
1.41	1 M 2C	19.9	199	75	41.9	57	30.5	–	0.93	0.00	0.00	0.93	0.93	0.65	2.63	0.83	0.08	0.018
1.56	1 M 2D	20.9	209	67	47.2	71	26.8	4.35	1.02	0.00	0.00	1.02	0.83	0.66	3.10	0.81	0.09	0.021
1.71	1 M 2E	18.6	186	70	36.7	96	25.9	–	1.09	0.00	0.00	1.09	0.55	0.72	5.11	0.73	0.08	0.025
2.08	IM 4A	19.5	195	60	32	43	19.9	–	1.58	0.00	0.00	1.58	0.85	0.61	5.98	0.70	0.07	0.018
6.89	IM 11A	30.9	309	69	46.2	127	20.5	–	1.18	0.01	0.08	1.17	0.38	0.68	10.48	0.65	0.05	0.018
7.09	IM 11B	16.1	161	69	30.7	67	11.4	5.1	1.40	0.00	0.00	1.40	0.23	0.79	5.72	0.80	0.07	0.018
7.29	IM 11C	30.3	303	93	39.5	125	54.8	–	0.95	0.01	0.08	0.94	1.00	0.62	7.12	0.71	0.10	0.029
7.62	IM 13A	23.8	238	70	26.8	106	21.3	–	1.22	0.01	0.08	1.21	0.36	0.98	11.74	0.64	0.08	0.032
7.82	1 M 13B	18.2	182	84	29.2	94	14.4	–	1.28	0.00	0.00	1.28	0.30	0.77	4.32	0.81	0.07	0.021
8.03	IM 14A	23.1	231	99	38.8	191	64.8	–	1.23	0.01	0.08	1.22	1.05	0.85	7.78	0.70	0.10	0.028
8.73	IM 16A	13.4	134	76	25.9	128	30.6	–	1.18	0.00	0.00	1.18	0.52	1.00	32.02	0.47	0.10	0.037
8.98	IM 16B	13.2	132	88	31	122	62.2	–	1.54	0.03	0.25	1.51	1.02	0.96	14.25	0.65	0.11	0.034
9.23	1 M 16C	13.3	133	86	33.7	69	31.9	–	1.34	0.00	0.00	1.34	0.69	0.86	7.04	0.77	0.12	0.028
9.48	1 M 16D	17.9	179	90	23.4	38	18.1	–	1.11	0.01	0.08	1.10	0.46	0.84	4.96	0.81	0.11	0.026
9.87	IM 18a	22.6	226	276	27.1	47	57.6	–	0.33	0.01	0.08	0.32	1.17	1.01	2.09	0.93	0.11	0.014
10.33	IM 18C	15.3	153	121	47	34	14.7	–	0.62	0.01	0.08	0.61	0.45	1.00	2.03	0.92	0.05	0.011
10.5	IM 19A	14.2	142	124	41.9	37	18.3	–	0.84	0.01	0.08	0.83	0.65	0.96	3.05	0.89	0.07	0.015
10.64	IM 19B	13	130	104	34	32	11.9	–	0.81	0.01	0.08	0.80	0.28	0.92	4.08	0.87	0.07	0.015
10.92	IM 19D	14.2	142	107	46.3	33	13.9	–	1.03	0.00	0.00	1.03	0.26	1.03	5.24	0.82	0.06	0.013
11.06	IM 19E	10.1	101	87	38.1	30	7.9	–	1.18	0.03	0.25	1.15	0.29	0.85	2.57	0.90	0.06	0.014
1.11	IM 2A	14	140	140	33.7	30	16.3	–	1.10	0.00	0.00	1.10	0.56	0.77	4.02	0.80	0.06	0.014
2.24	IM 4B	11.2	112	23	12	39	19.9	–	0.91	0.08	0.69	0.83	2.62	1.00	15.76	0.39	0.05	0.015

Table 1 (continued)

Depth (m)	Mamu	Th	Th*10	Sr	Pb	Zn	Y	pH	TC	TIC	% calcite	TOC	Y/Ni	Cr/V	Fe/Ti	Al/(Fe + Al + Mn)	K/Al	Mg/Al
8.23	IM 14B	17.9	179	90	23.4	38		–	1.15	0.01	0.08	1.14			4.96	0.81	0.11	0.024
8.43	IM 14C	16.2	162	89	37.7	128	36.7	–	1.25	0.00	0.00	1.25	0.49	0.90	11.62	0.67	0.09	0.031
10.13	IM 18B	14.2	142	107	46.3	33	10.5	–	1.10	0.00	0.04	1.10	0.19	1.03	2.22	0.91	0.06	0.013
	Mean	17.64	176.37	96.07	34.86	69.89	26.16	4.73	1.40	2420.67	0.10	1.09	0.65	0.85	7.02	0.76	0.08	0.021
	SD	5.14	51.39	43.26	8.66	43.64	16.31	0.53	1.11	1152.22	0.18	0.27	0.49	0.15	6.23	0.13	0.02	0.007
4.28	OK 7A	26.4	264	72	46.6	80	36.9	–	2.52	0	0	2.52	1.09	0.97	3.83	0.77	0.04	0.011
4.5	OK 7B	24.5	245	47	23.7	174	32.1	–	0.99	0.03	0.28	0.95	1.49	1.71	4.42	0.71	0.03	0.009
4.72	OK 7C	19.2	192	73	71	96	39.8	5.08	2.36	0.01	0.08	2.35	0.61	0.89	12.59	0.69	0.03	0.008
4.94	OK 7D	20.5	205	78	52.7	118	43.3	-	2.86	0.00	0.00	2.86	0.76	1.12	8.29	0.75	0.03	0.007
5.16	OK 7E	19.3	193	79	48.7	145	32.7	5.05	2.96	0.00	0.00	2.96	0.74	0.90	2.52	0.85	0.03	0.006
5.38	OK 7F	11.9	119	62	34.6	149	14	–	2.19	0.00	0.00	2.19	0.16	0.73	2.67	0.88	0.03	0.006
5.6	OK 7G	26	260	74	35	29	21.4	–	2.49	0.01	0.08	2.48	0.41	0.67	2.52	0.85	0.05	0.007
5.82	OK 7H	20	200	57	29.3	30	12.8	–	2.60	0.01	0.08	2.59	0.48	1.45	1.45	0.90	0.03	0.006
6.04	OK 7I	17.3	173	70	46.9	37	10.1	–	1.78	0.00	0.00	1.78	0.38	1.04	1.59	0.91	0.03	0.005
6.28	OK 7 J	25.7	257	76	47.7	31	17.2	–	1.83	0.01	0.08	1.82	0.59	1.14	1.55	0.88	0.04	0.006
7.25	OK 9	19.6	196	73	41.1	33	13.2	5.24	0.47	0.23	1.91	0.24	0.28	1.00	1.04	0.95	0.03	0.005
7.74	OK 11A	14.8	148	75	36.4	31	13.9		0.72	0.02	0.20	0.70	0.55	1.02	1.74	0.89	0.05	0.008
7.94	OK 11B	14.4	144	80	42.9	28	14.1	5.32	0.42	0.00	0.00	0.42	0.64	0.85	1.48	0.90	0.07	0.012
9.36	OK 13A	20.5	205	63	38.4	30	16.7	–	0.92	0.00	0.00	0.92	0.66	1.15	1.42	0.90	0.04	0.006
9.63	OK 13B	13.3	133	65	49	37	13.2	–	1.36	0.07	0.56	1.30	0.45	0.98	1.12	0.92	0.04	0.006
10.3	OK 15	36.4	364	70	36.8	18	24.1	–	0.38	0.00	0.00	0.38	0.88	1.04	0.67	0.92	0.07	0.007
10.5	OK 17	35.1	351	70	34.9	23	21.3	–	1.04	0.00	0.00	1.04	0.50	1.38	0.80	0.93	0.05	0.005
10.8	OK 19A	23.8	238	61	37.7	31	18.9	–	1.17	0.01	0.08	1.16	0.63	1.26	0.69	0.95	0.03	0.005
11.3	OK 19B	19.7	197	73	47.5	37	14.6	–	0.69	0.01	0.08	0.68	0.41	1.14	1.01	0.93	0.03	0.006
11.95	OK 21A	35.3	353	95	41.6	23	27.9	–	0.28	0.01	0.08	0.27	1.16	0.77	1.04	0.89	0.06	0.009
12.33	OK 21B	28	280	102	40.7	23	23.1	–	0.41	0.01	0.08	0.40	1.04	0.93	1.44	0.87	0.06	0.010
14.62	OK 24A	15.9	159	59	42.5	30	20.6	–	1.37	0.00	0.00	1.37	0.61	1.13	0.66	0.95	0.03	0.005
15.01	0 k 24B	25.2	252	51	43.4	19	20.5	–	0.59	0.00	0.00	0.59	0.79	1.04	0.74	0.93	0.05	0.005
	Mean	22.30	222.96	70.65	42.13	54.43	21.84	5.17	1.41	0.02	0.16	1.39	0.66	1.06	2.40	0.87	0.04	0.007
	SD	6.88	68.75	12.42	9.30	47.47	9.40	0.13	0.89	0.05	0.40	0.91	0.31	0.24	2.79	0.08	0.01	0.002
Mamu Av		19.78	197.80	84.38	38.21	62.78	-	5.02	1.25	0.02	0.13	1.23	0.66	0.95	4.90	0.81	0.06	0.014
63	OB 1	13.50	135.00	204.00	35.80	130.00	36.90	5.87	3.40	0.14	1.17	3.26	0.46	1.48	9.72	0.55	0.14	0.09
125	OB 2	12.50	125.00	324.00	25.00	120.00	38.50	–	2.28	1.48	12.33	0.80	0.55	1.00	9.68	0.57	0.08	0.13
195	OB 3	11.00	110.00	367.00	25.50	130.00	37.10	5.99	1.92	0.78	6.50	1.14	0.37	0.98	13.87	0.50	0.09	0.15
265	OB 4	10.60	106.00	332.00	24.60	120.00	40.80	5.96	0.00	–	–	0.00	0.45	1.07	9.75	0.59	0.10	0.27
395	OB 5	11.70	117.00	304.00	21.70	110.00	29.60	5.96	1.20	0.21	1.75	0.99	0.42	1.25	9.53	0.61	0.10	0.21

Table 1 (continued)

Depth (m)	Mamu	Th	Th*10	Sr	Pb	Zn	Y	pH	TC	TIC	% calcite	TOC	Y/Ni	Cr/V	Fe/Ti	Al/(Fe + Al + Mn)	K/Al	Mg/Al
465	OB 6	12.60	126.00	273.00	23.40	120.00	33.70	5.91	0.00	–	–	0.00	0.56	0.91	8.83	0.65	0.09	0.16
565	OB 7	9.80	98.00	331.00	18.80	90.00	28.20	5.91	2.52	1.37	11.41	1.15	0.56	0.98	9.47	0.62	0.10	0.28
675	OB 8	10.40	104.00	353.00	18.70	100.00	39.90	5.93	1.15	0.24	2.00	0.91	0.67	1.16	10.73	0.59	0.11	0.27
745	OB 9	10.10	101.00	356.00	21.40	110.00	27.70	5.90	2.15	0.42	3.50	1.73	0.40	1.03	9.74	0.63	0.11	0.35
815	OB 10	11.30	113.00	305.00	22.20	100.00	29.80	5.91	0.00	-	-	0.00	0.37	0.90	9.00	0.64	0.13	0.21
865	OB 11	10.30	103.00	307.00	21.10	110.00	31.60	5.90	1.63	0.48	4.00	1.15	0.40	1.08	10.80	0.60	0.13	0.23
1085	OB 12	7.90	79.00	264.00	33.50	110.00	29.70	–	4.19	1.59	13.24	2.60	0.42	0.93	12.87	0.55	0.13	0.24
1115	OB 13	9.90	99.00	323.00	33.80	90.00	37.80	5.90	1.46	0.32	2.67	1.14	0.27	1.00	9.47	0.62	0.11	0.25
	Mean	10.89	108.92	311.00	25.04	110.77	33.95	5.92	1.68	0.70	5.86	1.14	0.45	1.06	10.27	0.60	0.11	0.22
	SD	1.46	14.60	44.05	5.73	13.20	4.73	0.03	1.28	0.57	4.72	0.96	0.11	0.16	1.50	0.04	0.02	0.07
35	EG 1	9.80	98.00	151.00	21.30	70.00	34.10	–	1.53	1.42	11.83	0.11	0.85	1.05	6.96	0.44	0.13	0.54
55	EG 2	6.80	68.00	377.00	19.90	80.00	17.80	–	0.00	–	–	–	0.36	1.21	12.16	0.44	0.13	0.74
100	EG 3	8.40	84.00	190.00	26.40	120.00	73.10	-	0.00	–	–	–	1.46	0.89	12.18	0.39	0.08	0.50
125	EG 4	5.40	54.00	466.00	25.70	130.00	48.20	5.94	0.00	–	–	–	0.96	1.03	36.28	0.31	0.12	2.36
165	EG 5	8.60	86.00	247.00	17.80	100.00	30.00	-	0.00	–	–	–	0.75	1.15	10.31	0.40	0.13	0.72
175	EG 6	10.30	103.00	331.00	22.70	100.00	44.30	5.94	2.23	1.98	16.49	0.25	0.89	0.94	11.55	0.35	0.13	0.50
205	EG 7	10.90	109.00	271.00	21.30	100.00	40.80	5.93	1.34	0.77	6.41	0.57	0.82	0.92	10.65	0.34	0.17	0.60
235	EG 8	10.70	107.00	257.00	23.50	100.00	33.20	5.88	3.43	1.72	14.33	1.71	0.66	0.96	11.79	0.32	0.16	0.69
275	EG 9	7.90	79.00	310.00	17.50	80.00	45.00	5.93	1.75	1.70	14.16	0.05	0.90	0.87	30.28	0.25	0.13	1.08
295	EG 10	4.60	46.00	469.00	13.40	100.00	40.80	–	0.00	–	–	–	1.02	1.10	43.67	0.31	0.16	2.43
	Mean	8.34	83.40	306.90	20.95	98.00	40.73	5.92	1.03	1.52	12.64	0.54	0.87	1.01	18.58	0.35	0.13	1.02
	SD	2.20	21.95	106.68	3.97	18.14	14.44	0.03	1.22	0.46	3.85	0.69	0.28	0.12	13.01	0.06	0.03	0.75
Imo Fm. Av		9.78	97.83	309.22	23.26	105.22	36.90	5.92	1.40	0.97	8.12	0.98	0.63	1.04	13.88	0.01	0.12	0.57
WSA		3.7	37	300	22	95	26	–	–	–	–	0.2	0.38	0.69	11.40	0.62	0.34	0.18

WSA = World Shale Average (Wedepohl 1971, 1991)

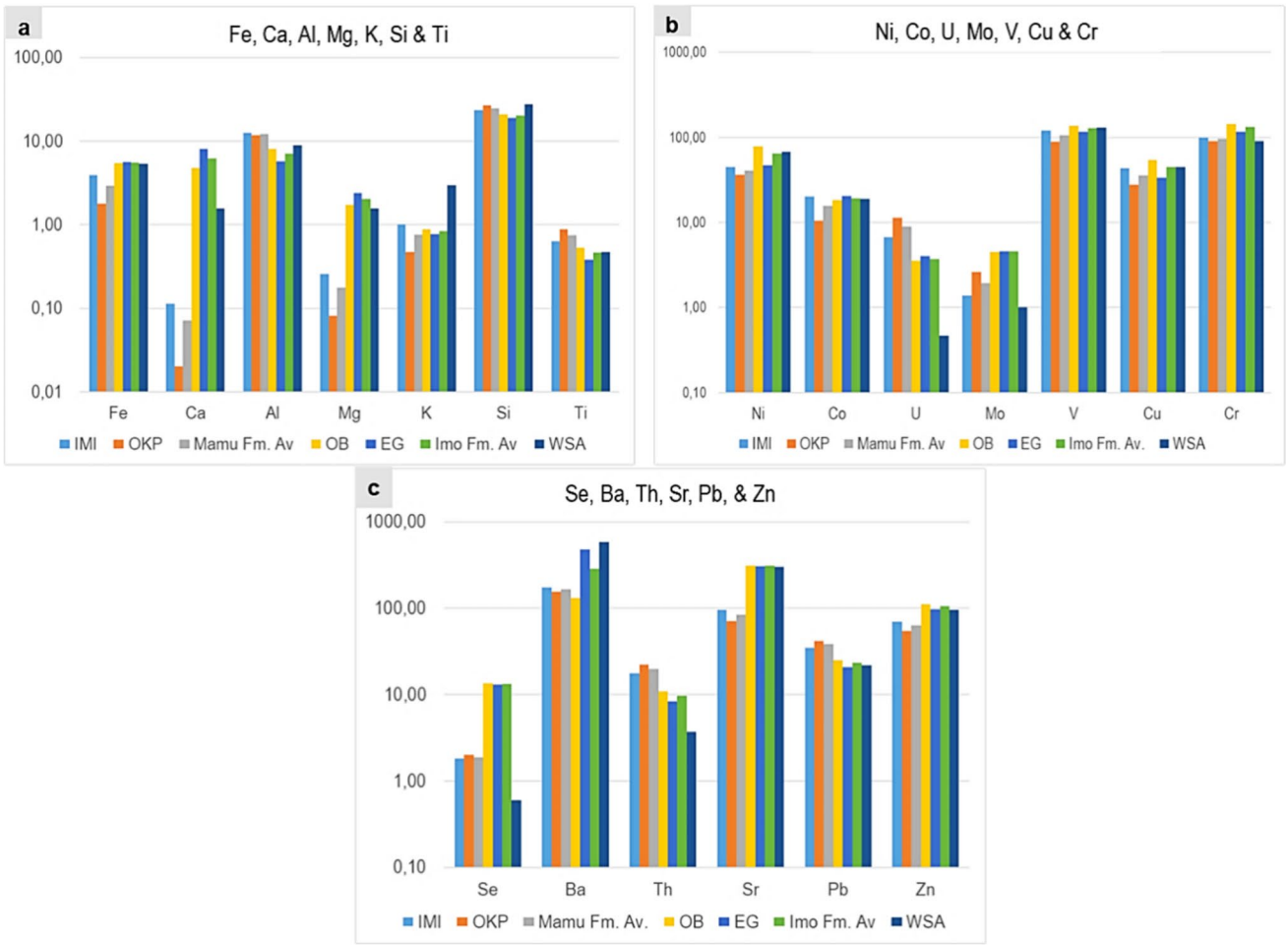

Fig. 4 **a**-**c** Comparison of World Shale Average (Wedepohl 1971, 1991) with mean concentrations of major and trace elements recorded from the Mamu and Imo formation mudrock samples

4.3 Trace metals

4.3.1 Redox-sensitive trace elements (RSTE)

4.3.1.1 Imo Formation The mean values of the RSTE recorded from the Imo Formation calcareous mudrocks are 64.78 ppm, 19.26 ppm, 3.75 ppm, 128.17 ppm, 131.74 ppm, 4.57 ppm, 45.17 ppm, for Ni, Co, U, V, Cr, Mo, and Cu, respectively (Fig. 4b). Excluding, Ni, V, and Cu, the mean concentration of other RSTE are higher than their corresponding WSA values, Ni = 68 ppm, Co = 19 ppm, U = 3.7 ppm, V = 130 ppm, Cr = 90 ppm, Mo = 1 ppm, and Cu = 60 ppm, (Wedepohl 1971, 1991), (Fig. 4b). Apart from V and Cr, which show a general increase towards the top section, the others show no noticeable trend in the OB well. The EG well calcareous mudrock samples show more variability in RSTE when compared to the OB calcareous mudrock samples (Fig. 3c-d). Observed data reveal uniform Ni, Mo, and U concentrations from bottom to top. Higher Cr and V concentrations were recorded at the bottom section, whereas Co and Cu show a general increase in concentration towards the top section. Overall, the Imo Formation calcareous mudrocks exhibit higher Ni, Co, V, Cr, Mo, and Cu concentrations than the dark estuarine mudrock samples, which show higher U concentrations (Fig. 4b).

4.3.1.2 Mamu Formation The mean values of the RSTE recorded from the Mamu Formation dark mudrock samples are 40.99 ppm, 15.72 ppm, 8.91 ppm, 106.10 ppm, 95.82 ppm, 1.95 ppm, and 36.10 ppm for Ni, Co, U, V, Cr, Mo, and Cu, respectively (Fig. 4b). While the mean U, Cr, and Mo concentrations in the dark mudrock samples exceed the WSA values, the mean Ni, Co, V, and Cu concentrations are lower than the WSA (Fig. 4b). In the OKP location, the Mo, Ni, V, Cr, and Co concentration gradually decreases towards the top section, which is unlike the U and Cu concentration, which show an overall increase towards the top. In general, the dark mudrock samples from the OKP loca-

tion show greater variability in Mo, Ni, Co, U, and Cr concentrations when compared with the samples from the IMI location, that show greater variability in V and Cr concentrations.

4.3.2 Se, Pb, Zn, Ba, Sr, and Th

4.3.2.1 Imo Formation The mean concentrations of Se, Pb, Zn, Ba, Sr, and Th recorded from the Imo Formation calcareous mudrocks are 13.35 ppm, 23.26 ppm, 105.22 ppm, 284.30 ppm, 309.22 ppm, and 9.78 ppm, respectively (Fig. 4c). The mean concentrations of Pb, Zn, Sr, Se and Th measured from the calcareous mudrocks are higher than those of the corresponding WSA [(Pb = 22 ppm, Zn = 95 ppm, Sr = 300 ppm, Se = 0.6 ppm, and Th = 3.7 ppm (Wedepohl 1971, 1991), while the mean Ba concentration is lower than the WSA for Ba (580 ppm, Wedepohl 1971 1991) (Fig. 4c) The calcareous mudrock samples from the OB well show greater variability in Se, Ba, Pb, Zn, and Sr when compared with samples from the EG well.

In addition, excluding Pb, the mean Se, Zn, Ba, and Sr values recorded from the Imo Formation calcareous mudrocks are significantly higher than those recorded from the Mamu Formation dark mudrock samples (Fig. 4c), which show higher Th concentration.

4.3.2.2 Mamu Formation The mean concentrations of Se, Pb, Zn, Ba, Sr, and Th recorded from the Mamu Formation dark mudrock samples are 1.88 ppm, 38.21 ppm, 62.78 ppm, 165.20 ppm, 84.38 ppm, and 19.78 ppm, respectively. Similarly, except for Pb and Th, which are higher than the WSA value, the dark mudrock samples are depleted in Zn, Ba, and Sr below the WSA (Fig. 4c). Furthermore, the dark mudrock samples from IMI show greater variability in Sr and Ba when compared with the OKP dark mudrock samples that show greater variability in Se, Pb, and Zn.

4.4 TOC, TIC, and pH

The Imo Formation calcareous mudrocks show a higher pH (mean pH of 5.92) when compared with the Mamu Formation dark mudrock samples (mean pH of 5.02). Similarly, the mean TIC and calcite percentage values from the Imo Formation calcareous mudrock samples are higher (0.97 wt% and 8.12%, respectively) than those obtained from the Mamu Formation mudrock samples (0.02 wt% and 0.13%, respectively). Conversely, the Mamu Formation samples show greater mean TOC and organic matter percentages (TOC*1.724) (1.23 wt% and 2.12 wt%, respectively) than the Imo Formation calcareous mudrocks (0.98 wt% and 1.68 wt%, respectively).

5 Discussion

5.1 Palaeodepositional processes

Facies analysis conducted on the IMI and OKP sections reveals two facies associations: Marsh/bay/central basin-beach-barrier/washover fan, and Fluvial-tidal channel lithofacies associations. The facies associations depict deposition under wave-dominated tide influenced by an estuarine setting. More detailed discussion is provided in Edegbai et al. (2019). The dark mudrock facies, from which the samples for this study are derived, depict brackish estuarine gross palaeodepositional environments (Edegbai et al. 2019). The facies succession of the EG and OB wells shows deepening water depth under widespread flooding. Insight from unpublished palynological data, uninterrupted thickness of the mudrocks (varying from 270ft to > 1000ft), together with sedimentological analysis of the sands (Edegbai and Ehigie 2024), depict deposition in a shallow marine shelf paleoenvironment.

5.2 Provenance and paleoclimate controls on Se concentration

The Cr/V versus (vs.) Y/Ni cross plot (Fig. 5) illustrates a dominantly felsic detrital provenance for the Imo Formation calcareous mudrock samples and the dark estuarine mudrock samples. Notwithstanding the similar provenance and climate (Hay and Floegel 2012; Boucot et al. 2013), our data show greater Se concentration in the calcareous mudrocks of the Imo Formation, especially in the EG well, where up to 21 ppm was recorded (Table 1). Higher Se concentration correlates with increasing mafic content of rocks (Malisa 2001). The mean Cr and Ni data recorded for the Imo Formation calcareous mudrocks are higher than the dark estuarine mudrocks samples (Sect. 4.3; Table 1). Some Palaeocene calcareous mudrock samples' Cr and Ni data are at or slightly above the threshold of 150 ppm and 100 ppm, which is characteristic of less felsic detrital source rocks (Table 1). The foregoing is supported by deduction from the V-Ni-Th*10 ternary plot (Fig. 5b) (Bracciali et al. 2007), together with a positive covariation of Cr, Ni *vs.* Al (Fig. 6b-e). Consequently, it is hypothesized that the Imo Formation calcareous mudrock samples show a substantial detrital contribution for Cr and Ni from intermediate – mafic provenance when compared with the dark estuarine mudrock samples.

5.3 TOC, proximality, and paleoredox controls on Se concentration

Being a chalcophile element, Se is commonly associated with Zn and Pb (Emsley 2011) and can also be sequestered

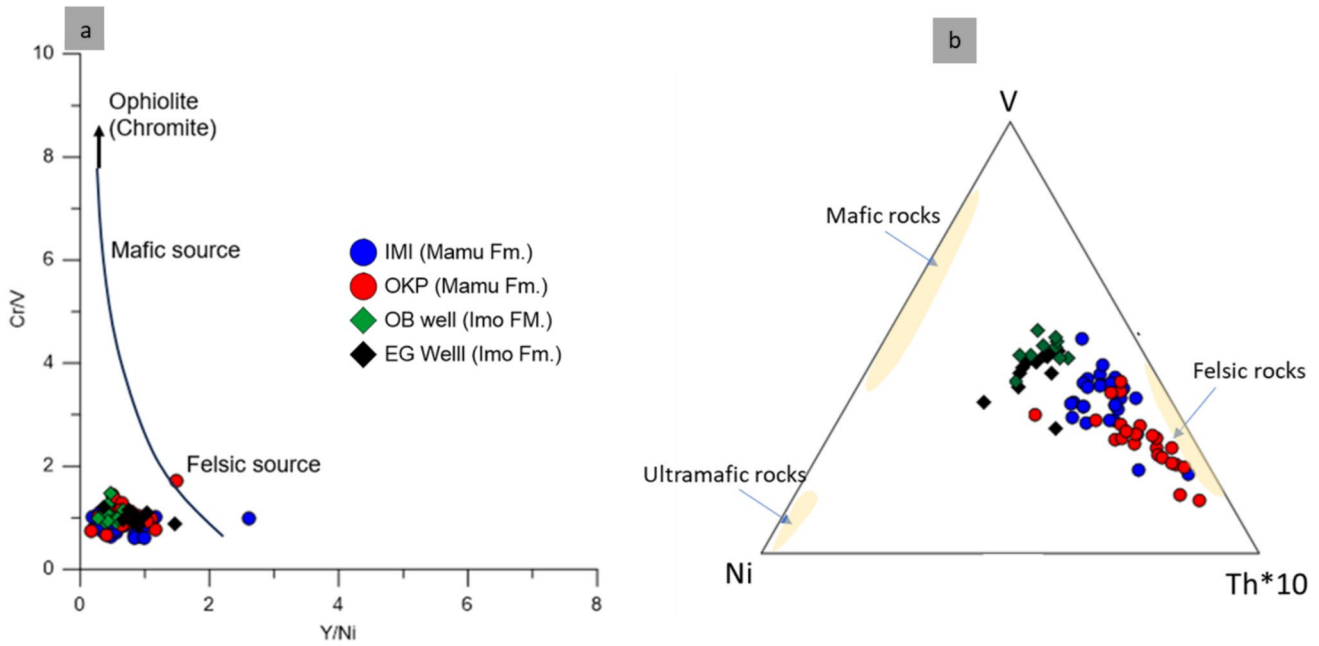

Fig. 5 **a** Provenance discriminant plot depicting the predominant felsic provenance (Hiscott 1984); **b** V-Ni-Th*10 ternary plot suggesting significant detrital contribution from intermediate sources in the Palaeocene (Bracciali et al. 2007)

by organic matter under reducing conditions. The weak to broad covariation of Se with TOC shows that organic matter was not important in sequestering Se in the Imo and Mamu Formation, especially in the proximal IMI and EG locations (Fig. 6b-e).

Bottom water anoxia facilitates the sequestration of redox-sensitive trace metals. Crossplots of molybdenum versus uranium enrichment factor, together with crossplots of TOC versus RSTE are important trackers of bottom water oxygen levels (Tribovillard et al. 2006, 2012; Algeo and Li 2020). The Palaeogene samples show strong positive covariation between the enrichment factors of molybdenum and uranium, which contrasts with the broad distribution observed in the Maastrichtian samples. The foregoing illustrates sequestration of authigenic uranium and molybdenum in suboxic to anoxic bottom waters during the Palaeogene flooding episode. The moderate to strong covariation of Mo, U, Ni, Cu, Cr, Zn, and Pb with TOC suggests some level of anoxia (dysoxic to anoxic) was prevalent in the pore waters at the proximal EG well (Imo Formation), as well as in the OKP and IMI locations (Mamu Formation) (Fig. 6d, e). Additionally, Se covariates moderately to strongly with chalcophile (Pb and Zn) and siderophile (Fe, Co, Ni, and Mo) elements in the EG and OKP wells (Fig. 6d, e), which illustrates the role of reducing conditions in the bottom waters in sequestering Se around the OKP and EG wells. Furthermore, the strong Fe *vs.* Se covariation suggests that Fe-minerals (perhaps pyrite) are important Se sorption sites in the OKP location. Principal component analysis (PCA) show positive loadings for Mg, Ca, Se, TIC and % calcite on PC1 and PC2. Conversely, negative loadings were recorded for Th, Si, Al, Ti, and TOC for PC1, with Co, Al, V, Ni and Cr reported for PC2, respectively. The PC1 biplot (58.2% of total variance) show vectors associated with carbonate minerals and Se pointing in same direction, which contrasts the vectors associated with grainsize and provenance. Furthermore, PC2 (15.6% of total variance) PC2 captures the variation in the association of clay + redox-sensitive/trace metals and organic matter relative to the quartz + carbonate framework. The foregoing favours a strong association of Se with carbonate minerals.

5.4 Water depth, paleosalinity, hydrothermal influence, nature of clay minerals, and pH controls on Se concentration

The Se concentration in saline water shows a direct relationship with water depth (Xu et al. 2024). Being a bio-limited element, Se is assimilated by bacteria and phytoplankton in the photic zone (Duan et al. 2010). However, at depth, bioproductivity reduces, leading to a gradual recovery of the Se concentration, which is enhanced by Se release from decaying organic matter (Zhou et al. 2019). The concentrations and ratios of major elements are also instructive in deducing paleosalinity conditions and hydrothermal influence. The Imo Formation calcareous mudrock samples are inferred to have

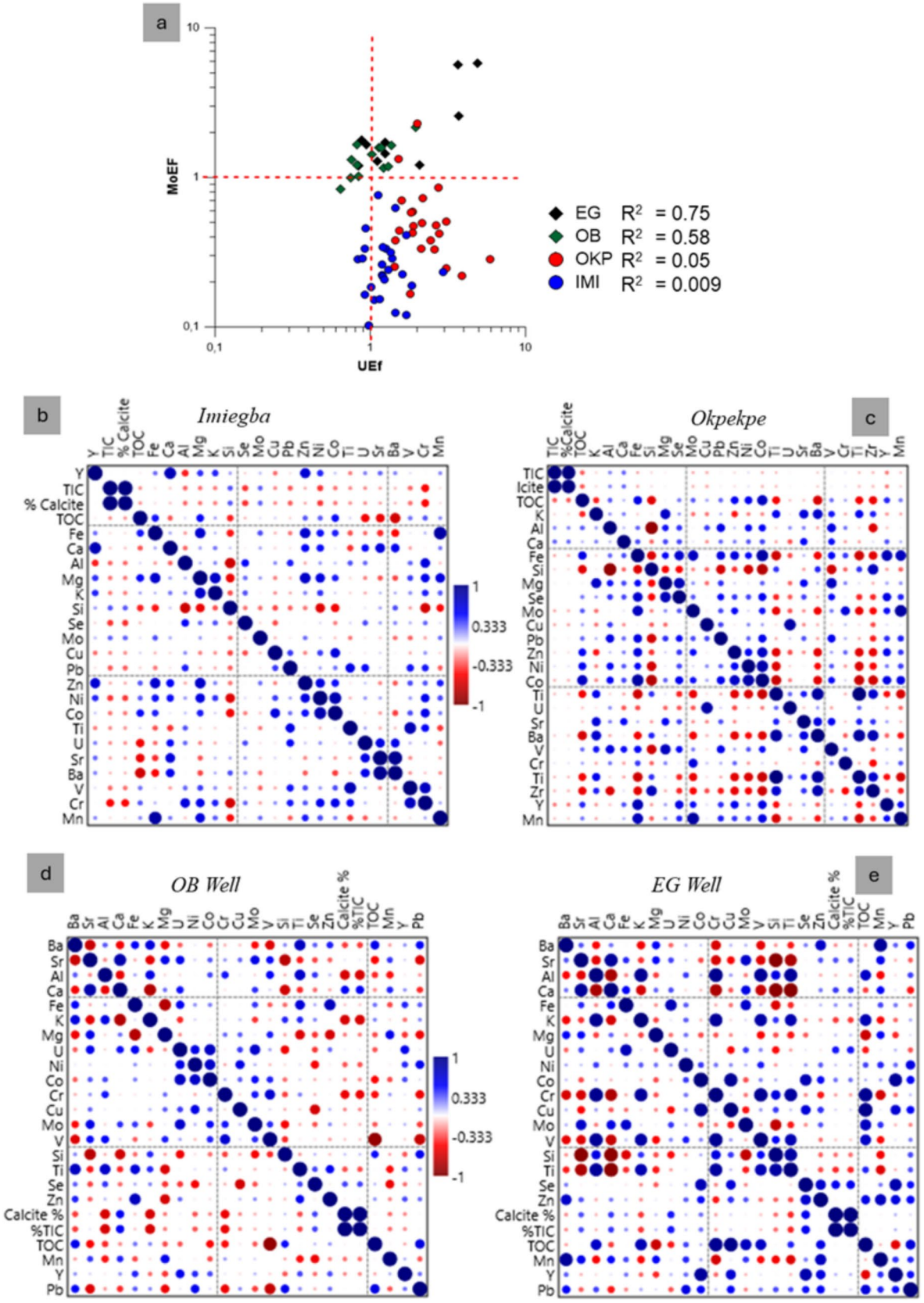

Fig. 6 **a** MoEf vs UEf binary plot, **b-e** Correlation charts for the dark estuarine mudrock samples (IMI and OKP sections) and calcareous marine mudrock samples (OB and EG wells)

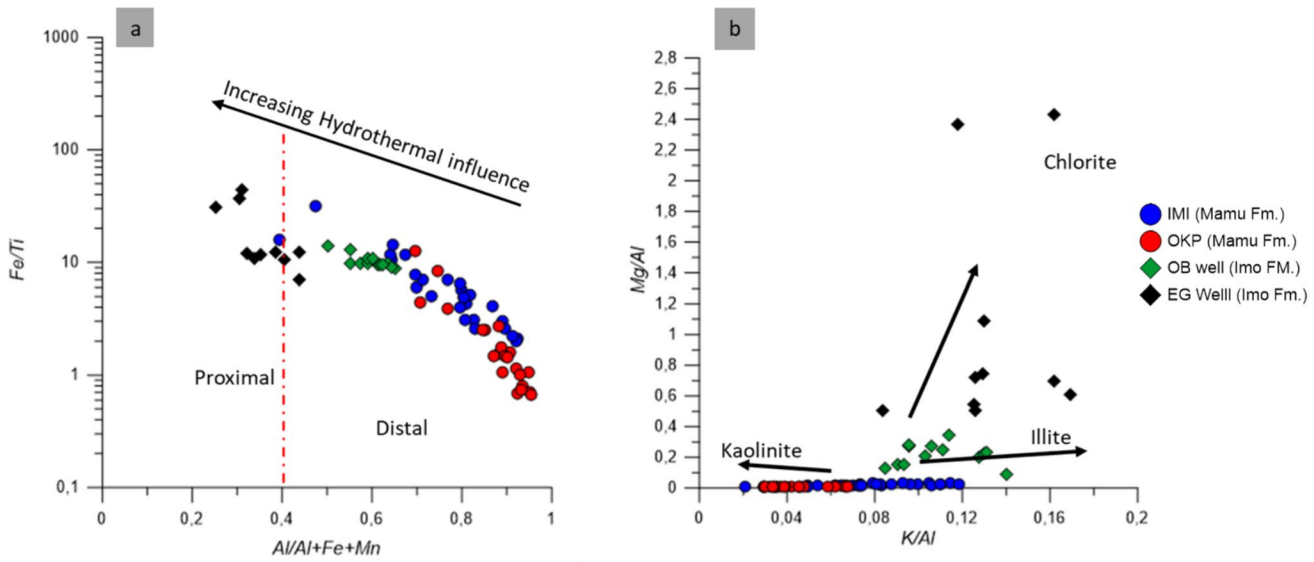

Fig. 7 **a** Fe/Ti versus Al/Al + Fe + Mn plot illustrating stronger hydrothermal influence on the Imo Formation calcareous mudrocks (modified from Olatunde Popoola et al. 2019); **b** Mg/Al versus K/Al discriminant plot showing greater illite and chlorite content in the Imo Formation mudrocks (Turgeon and Brumsack 2006)

been formed under higher salinity (marine conditions) with perhaps some hydrothermal influence based on the observed higher major element concentration and higher Mg/Al and K/Al concentrations (Table 1). This hypothesis is supported by the higher TIC, calcite content, Sr, and Ba concentrations recorded in the Imo Formation together with inferences from the Fe/Ti vs. Al/Al + Fe + Mn discriminant diagram (Fig. 7a, Olatunde Popoola et al. 2019). Additionally, the greater mudrock thickness recorded for the Imo Formation samples when compared with the Mamu Formation samples (Fig. 3a-d) suggests deposition in greater water depth during the Palaeocene marine transgression, which is postulated to account for higher Se concentration in the Imo Formation mudrock samples.

Clay minerals are also important in sequestering Se. Mixed and three-layered clays like illite, smectite, chlorite, etc. show better Se adsorption owing to their higher cation exchange capacity (Tian et al. 2016; Jamaluddin et al. 2024; Feng et al. 2024) than two-layered clays of the kandite group. The observed moderate positive Se *vs.* Al covariation illustrates Se sequestration on clay minerals (Fig. 6a–d). The higher K/Al recorded in the Imo Formation calcareous mudrock samples, alongside deductions from Mg/Al *vs.* K/Al (Fig. 7b) depict higher combined illite and chlorite

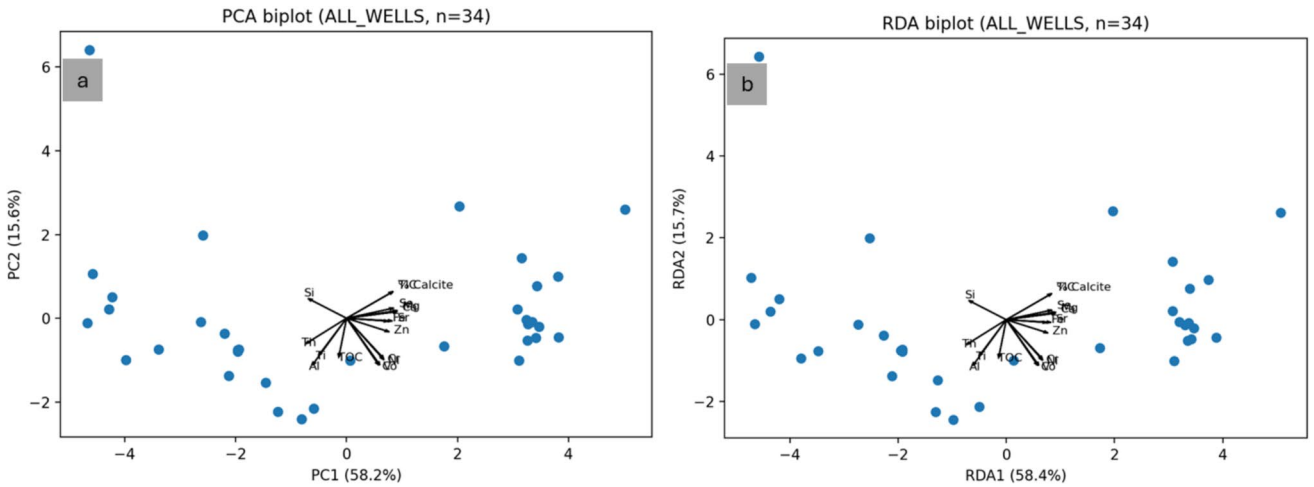

Fig. 8 **a-b** PCA and RDA plots for the Imo and Mamu formations mudrock samples illustrating a dominant carbonate control on selenium concentration

amounts when compared to the Mamu Formation dark mudrock samples, which possess a higher kaolinite content (Fig. 8). Mineralogical data on the dark estuarine mudrocks samples from a previous study show a higher kaolinite content that is at least twice that of the illite content (Appendices, Figs.9 and 10, Edegbai et al. 2019).

pH affects the solubility of selenide/selenate) (Fordyce 2012). Therefore, with increasing acidity, Se solubility increases. One should assume that the higher acidity (av. pH of 5.02) should facilitate better Se sequestration in the dark estuarine mudrocks. However, the opposite is true since the Imo Formation calcareous mudrocks with lower acidity (av. pH 5.92) show greater Se concentration by over one order. CO_3^{2-} from carbonates has been shown to promote Se adsorption under moderately acidic conditions (Wijnja and Schulthess 2002). This is hypothesized to have occurred in the Imo Formation calcareous mudrocks as illustrated by the moderate to strong positive TIC, calcite *vs.* Se covariation observed in the OB and EG wells (Fig. 6c-d). It is also worth noting that, much as SO_4^{2-} is enhanced under high salinity conditions, Fe is enhanced by hydrothermal activity (Fig. 7a).

Principal component analysis (PCA; Fig. 8a) was used to identify the dominant axes of natural covariance among selenium, carbonate indicators (Ca, Mg, Sr, TIC, %calcite), siliciclastic/provenance proxies (Al, Si, Ti, Th), redox-sensitive metals (Fe, Zn, Ni, Co, V, Cr), and total organic carbon (TOC). The first principal component explains approximately 58% of the variance and reflects a strong carbonate–siliciclastic contrast, with selenium loading together with Ca and Mg and opposite to provenance proxies. The second component (~ 16%) is dominated by redox-sensitive metals, indicating a secondary, orthogonal control distinct from carbonate content and provenance. Organic matter does not define a major axis of variability.

To explicitly test and quantify these controls, redundancy analysis (RDA; Fig. 8b) was conducted using carbonate, provenance, redox, and organic matter proxies as explanatory variables. The constrained ordination reproduces the structure observed in PCA, with selenium aligning strongly with carbonate proxies along the primary redundancy axis and redox-sensitive metals defining a secondary axis. The overall constrained model explains a large fraction of the multivariate variance and is statistically significant based on permutation testing, demonstrating that the selected geochemical proxies capture the dominant controls on selenium distribution.

Together, the PCA and RDA results show that selenium behavior is governed by separable carbonate, provenance, and redox influences, with carbonate content exerting the dominant control. The close alignment of selenium with Ca and Mg in both unconstrained and constrained ordinations indicates a shared carbonate-associated process rather than redundant correlation, thereby satisfying the requirement to separate co-varying controls.

5.5 Hypothesis on dietary intake of Se in the study area

The nature of underlying geology/soil and environmental factors like pH and prevailing weather conditions have been demonstrated to constrain the concentration of Se and other micronutrients in grains from South Africa, Ethiopia, and Malawi (Oldfield 1999; Van Ryssen 2006; Courtman et al. 2012; Gashu et al. 2021). Most rural dwellers are farmers and depend on homegrown food and water for their subsistence and dietary Se intake (Gashu et al. 2021). Aquifers interstratified within organic-rich mudrocks are known to possess a high content of heavy metals leached from the mudrocks (Zhang et al. 2022). In such occurrences, it is commonplace for groundwater in such regions to possess high Se concentration (Mayland et al. 1989; Kumar et al. 2011). Additionally, plants absorb Se in various redox states through the roots, which are subsequently transported alongside other minerals to the leaves and other parts of the plants through the xylem tissues. Studies have shown that root and tuber crops, especially yams, and cocoyam, which are staple foods, commonly possess higher Se than grains and vegetables (Gbadebo et al. 2010; Obahiagbon et al. 2011). Furthermore, meat from wild game (popularly called bush meat) and goat, which graze on grasses in the area, are important local sources of animal protein. From the foregoing, it is hypothesizedd that a higher background Se concentration, together with higher pH, will promote rapid absorption of Se by plants, and by animals and humans. Thus, it is herein hypothesized that food and water produced from areas underlain by the Imo Formation calcareous mudrocks will possess higher Se levels when compared with food grown from areas underlain by the Mamu Formation.

5.6 Wider implications and suggestions for further studies

The local geology, climate, and pH constrain the concentration of Se and other micronutrients. Marine mudrocks tend to possess higher Se content than non-marine mudrocks, as confirmed by this study. Additionally, Se is more likely to be bioavailable in marine mudrocks with higher pH compared to others. These deductions can be validated in other regions and geologic settings in a bid to shed light on the geospatial link with Se deficiency. Furthermore, an objective for further research will be to evaluate the Se concentration in tubers, grains, and vegetables and the controls of same from areas underlain by the Palaeogene calcareous marine mudrocks and the Upper Cretaceous dark estuarine mudrocks.

6 Conclusions

This study has shown that the concentration of Se in the Campanian–Maastrichtian and Palaeogene samples of the Mamu and Imo formations is higher than within the WSA. Data from this study shows that the Imo Formation calcareous mudrocks exhibit significantly higher Se concentrations compared to the dark estuarine mudrock units. This disparity is attributed to a significant detrital contribution from intermediate rocks with higher Se concentration, and deposition under a higher salinity marine paleoenvironment with hydrothermal influence. The foregoing is illustrated by higher major element concentrations, higher TIC and calcite concentrations, positive Cr and Ni covariation with Ti, the presence of illite and chlorite (from discriminant Mg/Al vs. K/Al), and Sr and Ba concentrations. It is also hypothesised that pH, dysoxic to anoxic paleoredox conditions, together with illite and chlorite clay minerals, enhanced Se adsorption onto clay and calcite mineral surfaces of the Imo Formation calcareous mudrocks.

Acknowledgements The first author thanks the University of Benin Research and Publications Committee and the Fulbright Commission (15160892) for contributing to his educational development over the years.

Author contributions Aitalokhai J. Edegbai: Conceptualization, Investigation, Methodology, Writing—original draft, Writing—review & editing. Jennifer B. Owonaro: Investigation, Methodology. Jubemi A. Pajiah: Writing—review & editing. Erepamo J. Omietimi: Writing—review & editing. Nils Lenhardt: Writing—review & editing.

Funding Open access funding provided by University of Pretoria. Fulbright Association, 15160892, Aitalokhai Edegbai

Declarations

Conflict of interest The authors declare that no known financial conflicts of interest or personal relationships could have influenced the work presented in this paper.

Appendix

See Fig. 9 and 10

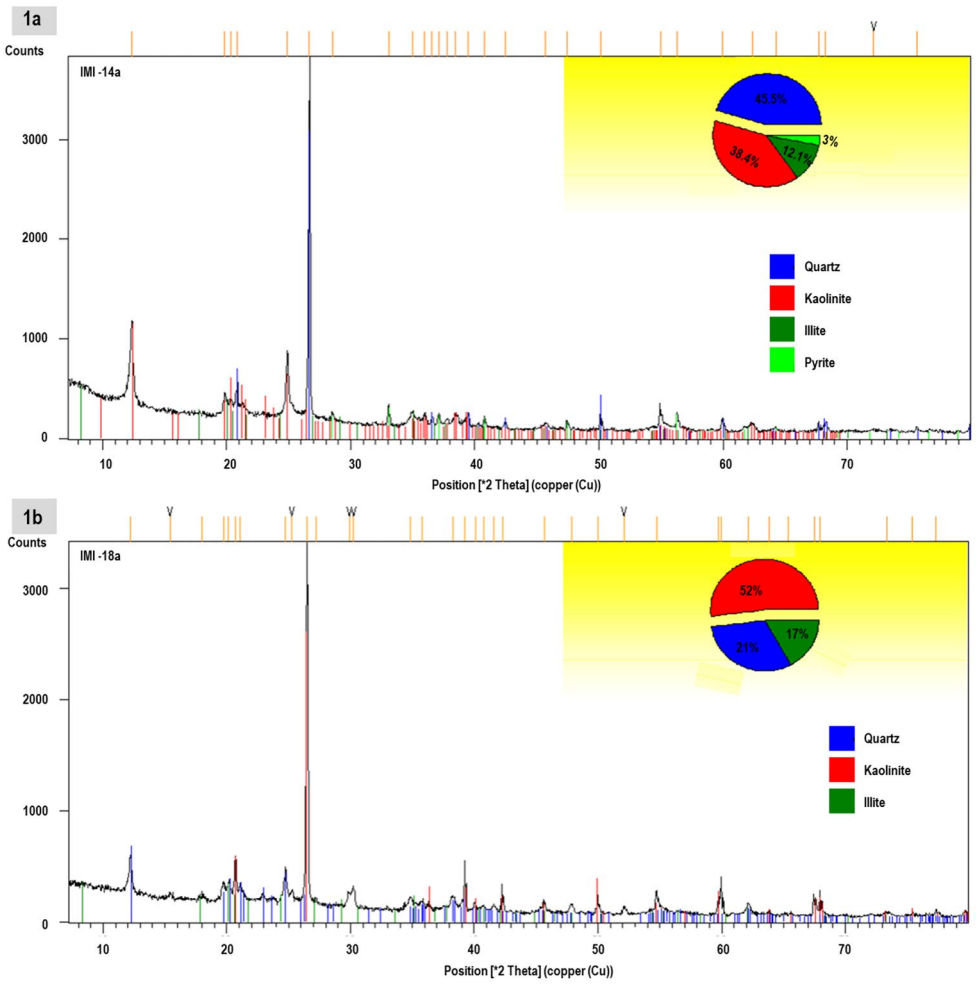

Fig. 9 X-ray diffractograms from the IMI locations

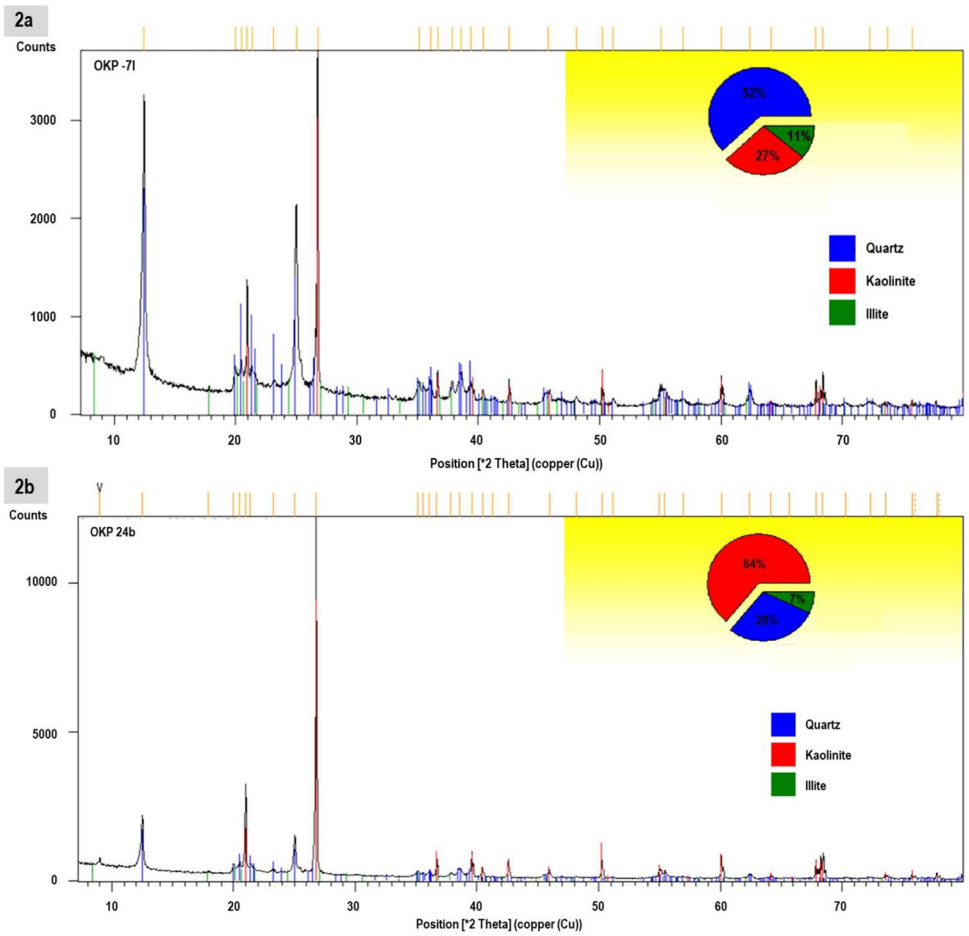

Fig. 10 X-ray diffractograms from the OKP locations

References

Abulude FO, Ogunkoya MO, Oroko TA (2006) Selenium in Nigeria Foods, Federal College of Agriculture. Akure pp 1–8

Adriano DC (2001) Trace Elements in Terrestrial Environments. Springer, New York, New York, NY. https://doi.org/10.1007/978-0-387-21510-5

Akande SO, Mücke A (1993) Depositional environment and diagenesis of carbonates at the Mamu/Nkporo formation, Anambra Basin, Southern Nigeria. J Afr Earth Sci Middle East 17(4):445–456. https://doi.org/10.1016/0899-5362(93)90003-9

Aremu MO, Atolaiye BO, Labaran L (2010) Environmental implication of metal concentrations in soil, plant foods and pond in area around the Derelict Udege mines of Nasarawa State, Nigeria. Bull Chem Soc Eth 24(3):351–360. https://doi.org/10.4314/bcse.v24i3.60666

Avbovbo AA (1978) Tertiary lithostratigraphy of Niger Delta. AAPG Bull 62(2):295–300

Benkhelil J (1989) The origin and evolution of the Cretaceous Benue trough (Nigeria). J Afr Earth Sci Middle East 8(2–4):251–282. https://doi.org/10.1016/s0899-5362(89)80028-4

Boucot AJ, Xu C, Scotese CR, Morley RJ (2013) Phanerozoic Paleoclimate: An Atlas of Lithologic Indicators of Climate. SEPM (Society for Sedimentary Geology), Tulsa, Oklahoma, U.S.A. https://doi.org/10.2110/sepmcsp.11

Bracciali L, Marroni M, Luca P, Sergio R (2007) Geochemistry and petrography of Western Tethys Cretaceous sedimentary covers (Corsica and Northern Apennines): From source areas to configuration of margins. In: Arribas J, Johnsson MJ, Critelli S (eds) Sedimentary Provenance and Petrogenesis: Perspectives from Petrography and Geochemistry. Geological Society of America, USA. https://doi.org/10.1130/2006.2420(06)

Courtman C, Van Ryssen J, Oelofse A (2012) Selenium concentration of maize grain in South Africa and possible factors

influencing the concentration. S Afr J Anim Sci 42(5):454–458. https://doi.org/10.4314/sajas.v42i5.2
Dhillon KS, Dhillon SK (2014) Development and mapping of seleniferous soils in northwestern India. Chemosphere 99:56–63. https://doi.org/10.1016/j.chemosphere.2013.09.072
Dim CIP, Mode AW, Okwara IC (2019) Signatures of key petroleum system elements: outcrop examples from the Anambra Basin, Southeastern Nigeria. J Pet Explor Prod Technol 9(3):1615–1631. https://doi.org/10.1007/s13202-018-0589-2
Dinh QT, Cui ZW, Huang J, Tran TAT, Wang D, Yang WX, Zhou F, Wang MK, Yu DS, Liang DL (2018) Selenium distribution in the Chinese environment and its relationship with human health: a review. Environ Int 112:294–309. https://doi.org/10.1016/j.envint.2017.12.035
Duan LQ, Song JM, Li XG, Yuan HM, Xu SS (2010) Distribution of selenium and its relationship to the eco-environment in Bohai Bay seawater. Mar Chem 121(1–4):87–99. https://doi.org/10.1016/j.marchem.2010.03.007
Edegbai AJ, Ehigie V (2024) Sedimentological aspects of subcropping sand units within Imo Formation, Western Niger Delta Basin. NIPES-J Sci Tech Res 6(1):234–244
Edegbai AJ, Schwark L, Oboh-Ikuenobe FE (2019) Campano-Maastrichtian paleoenvironment, paleotectonics and sediment provenance of western Anambra Basin, Nigeria: multi-proxy evidences from the Mamu Formation. J Afr Earth Sci 156:203–239. https://doi.org/10.1016/j.jafrearsci.2019.04.001
Eiche E, Bardelli F, Nothstein AK, Charlet L, Göttlicher J, Steininger R, Dhillon KS, Sadana US (2015) Selenium distribution and speciation in plant parts of wheat (*Triticum aestivum*) and Indian mustard (*Brassica juncea*) from a seleniferous area of Punjab, India. Sci Total Environ 505:952–961. https://doi.org/10.1016/j.scitotenv.2014.10.080
Ejezie F, Okaka A, Nwagha U (2012) Reduced maternal selenium levels in pregnant and lactating Nigerian women: should routine selenium supplementation be advocated. Niger J Med 21(1):98–102
Ekwenye OC, Nichols GJ, Collinson M, Nwajide CS, Obi GC (2014) A paleogeographic model for the sandstone members of the Imo Shale, south-eastern Nigeria. J Afr Earth Sci 96:190–211. https://doi.org/10.1016/j.jafrearsci.2014.01.007
Emsley J (2011) Nature's building blocks: An A-Z guide to the elements. Oxford University Press, USA
Eroglu C, Unal D, Cetin A, Orhan O, Sivgin S, Oztürk A (2012) Effect of serum selenium levels on radiotherapy-related toxicity in patients undergoing radiotherapy for head and neck cancer. Anticancer Res 32(8):3587–3590
Ezeama NN, Okunna N, Afonne OJ (2023) Dietary intake and status of selenium in breast milk and serum of lactating mothers in Awka, South East Nigeria. Nutr Health 31(2):527–536. https://doi.org/10.1177/02601060231195083
Fairweather-Tait SJ, Collings R, Hurst R (2010) Selenium bioavailability: current knowledge and future research requirements. Am J Clin Nutr 91(5):1484S-1491S. https://doi.org/10.3945/ajcn.2010.28674j
Favorito JE, Eick MJ, Grossl PR, Davis TZ (2017) Selenium geochemistry in reclaimed phosphate mine soils and its relationship with plant bioavailability. Plant Soil 418(1):541–555. https://doi.org/10.1007/s11104-017-3299-5
Feng CX, Liu S, Song WL, Hou CH, Yang YH (2024) Mineralogy and selenium speciation analysis of Early Cambrian selenium-rich black shale in southern Shaanxi Province, China. Minerals 14(6):612. https://doi.org/10.3390/min14060612
Finley JW (2006) Bioavailability of selenium from foods. Nutr Rev 64(3):146–151. https://doi.org/10.1111/j.1753-4887.2006.tb00198.x
Fisinin VI, Papazyan TT, Surai PF (2009) Producing selenium-enriched eggs and meat to improve the selenium status of the general population. Crit Rev Biotechnol 29(1):18–28. https://doi.org/10.1080/07388550802658030
Fordyce FM, Brereton N, Hughes J, Luo W, Lewis J (2010) An initial study to assess the use of geological parentmaterials to predict the Se concentration in overlying soils and in fi ve staple foodstuff s produced on them inScotland. Sci Total Environ 408(22):5295–5305. https://doi.org/10.1016/j.scitotenv.2010.08.007
Fordyce FM, Brereton N, Hughes J, Luo W, Lewis J (2010) An initial study to assess the use of geological parent materials to predict the Se concentration in overlying soils and in five staple foodstuffs produced on them in Scotland. Sci Total Environ 408(22):5295–5305. https://doi.org/10.1016/j.scitotenv.2010.08.007
Fordyce FM (2012) Selenium deficiency and toxicity in the environment. In: Selinus O et al (eds) Essentials of Medical Geology. Springer, Netherlands, pp 375–416. https://doi.org/10.1007/978-94-007-4375-5_16
Frankenberger WT Jr, Benson S (1994) Selenium in the Environment. CRC Press
Gashu D, Nalivata PC, Amede T, Ander EL, Bailey EH, Botoman L, Chagumaira C, Gameda S, Haefele SM, Hailu K, Joy EJM, Kalimbira AA, Kumssa DB, Lark RM, Ligowe IS, McGrath SP, Milne AE, Mossa AW, Munthali M, Towett EK, Walsh MG, Wilson L, Young SD, Broadley MR (2021) The nutritional quality of cereals varies geospatially in Ethiopia and Malawi. Nature 594(7861):71–76. https://doi.org/10.1038/s41586-021-03559-3
Gbadebo AM, Babalola OO, Ajigbotesho FL (2010) Selenium concentration in food and blood of residents of Abeokuta Metropolis, Southwestern Nigeria. J Geochem Explor 107(2):175–179. https://doi.org/10.1016/j.gexplo.2010.05.002
Gebhardt H (1998) Benthic foraminifera from the Maastrichtian lower Mamu Formation near Leru (southern Nigeria): paleoecology and paleogeographic significance. J Foraminiferal Res 28(1):76–89
Gebhardt H, Akande SO, Adekeye OA (2020) Cenomanian to Coniacian sea-level changes in the Lower Benue Trough (Nkalagu Area, Nigeria) and the Eastern Dahomey Basin: palaeontological and sedimentological evidence for eustasy and tectonism. Geol Soc Lond Spec Publ 498(1):233–255. https://doi.org/10.1144/sp498-2018-194
Hay WW, Floegel S (2012) New thoughts about the Cretaceous climate and oceans. Earth Sci Rev 115(4):262–272. https://doi.org/10.1016/j.earscirev.2012.09.008
Hiscott RN (1984) Ophiolitic source rocks for Taconic-age flysch: trace-element evidence. Geol Soc Am Bull 95(11):1261. https://doi.org/10.1130/0016-7606(1984)95%3c1261:osrftf%3e2.0.co;2
Jamaluddin SK, Wagreich M, Maria GS, Fathy D (2024) Effect of depositional environment and climate on organic matter enrichment in sediments of the upper Miocene: Pliocene kampungbaru formation, lower kutai basin. Indonesia Geosciences 14(6):164. https://doi.org/10.3390/geosciences14060164
Jimoh AA, Egbewande OO, Olorede BR, Hassan WA, Maigandi SA, Ibitoye EB (2024) Egg quality indices of black harco pullets fed nutraceuticals during hot-dry season in Sokoto metropolis. FUDMA J Agriculture and Agricultural Technol 10(1):117–124. https://doi.org/10.33003/jaat.2024.1001.15
Kieliszek M, Bano I, Zare H (2022) A comprehensive review on selenium and its effects on human health and distribution in middle eastern countries. Biol Trace Elem Res 200(3):971–987. https://doi.org/10.1007/s12011-021-02716-z

Kolawole SE, Obueh HO (2013) Relationship between soil contents and plasma levels of selenium, chromium and manganese in healthy adult Nigerians. Afr J Biotechnol 12(34):5339–5346. https://doi.org/10.5897/ajb12.107

Koljonen T (1973) Selenium in certain igneous rocks. Bull Geol Soc Finl 45(1):9–22. https://doi.org/10.17741/bgsf/45.1.002

Kumar AR, Riyazuddin P (2011) Speciation of selenium in groundwater: seasonal variations and redox transformations. J Hazard Mater 192(1):263–269. https://doi.org/10.1016/j.jhazmat.2011.05.013

Ladipo KO (1988) Paleogeography, sedimentation and tectonics of the upper Cretaceous Anambra basin, southeastern Nigeria. J Afr Earth Sci Middle East 7(5–6):865–871. https://doi.org/10.1016/0899-5362(88)90029-2

Latshaw JD, Osman M (1975) Distribution of selenium in egg white and yolk after feeding natural and synthetic selenium compounds. Poult Sci 54(4):1244–1252. https://doi.org/10.3382/ps.0541244

Lazar OR, Bohacs KM, MacQuaker JHS, Schieber J, Demko TM (2015) Capturing key attributes of fine-grained sedimentary rocks in outcrops, cores, and thin sections: nomenclature and description guidelines. J Sediment Res 85(3):230–246. https://doi.org/10.2110/jsr.2015.11

Lenhardt N, Omietimi EJ, Edegbai AJ, Schwark L, Catuneanu O, Fairhead JD, Götz AE (2025) Traversing the rift: a review of the evolution of the West and Central African Rift System and its economic potential. Earth Sci Rev 261:104999. https://doi.org/10.1016/j.earscirev.2024.104999

Ligowe IS, Phiri FP, Ander EL, Bailey EH, Chilimba ADC, Gashu D, Joy EJM, Lark RM, Kabambe V, Kalimbira AA, Kumssa DB, Nalivata PC, Young SD, Broadley MR (2020) Selenium deficiency risks in sub-Saharan African food systems and their geospatial linkages. Proc Nutr Soc 79(4):457–467. https://doi.org/10.1017/s0029665120006904

Lyons G, Stangoulis J, Graham R (2003) High-selenium wheat: biofortification for better health. Nutr Res Rev 16(1):45–60. https://doi.org/10.1079/nrr200255

Malisa EP (2001) The behaviour of selenium in geological processes. Environ Geochem Health 23(2):137–158. https://doi.org/10.1023/A:1010908615486

Mayland HF, James LF, Panter KE, Sonderegger JL (1989) Selenium in seleniferous environments. Selenium in Agriculture Environ 23:15–50

Measures CI, Burton JD (1980) The vertical distribution and oxidation states of dissolved selenium in the northeast Atlantic Ocean and their relationship to biological processes. Earth Planet Sci Lett 46(3):385–396. https://doi.org/10.1016/0012-821x(80)90052-7

Nganje TN, Edet A, Cuthbert S, Adamu CI, Hursthouse AS (2020) The concentration, distribution and health risk from potentially toxic elements in the soil - plant - water system developed on black shales in SE Nigeria. J Afr Earth Sci 165:103806. https://doi.org/10.1016/j.jafrearsci.2020.103806

Nigeria Geological Survey Agency (NGSA) (2022) The Geological map of Edo State. https://ngsa.gov.ng/wp-content/uploads/2024/08/Edo-State-Mineral-Resources-Map-2022.pdf

Nwagha UI, Ogbodo SO, Nwogu-Ikojo EE, Ibegbu DM, Ejezie FE, Nwagha TU, Dim CC (2011) Copper and selenium status of healthy pregnant women in Enugu, southeastern Nigeria. Niger J Clin Pract 14(4):408. https://doi.org/10.4103/1119-3077.91745

Nwajide CS (2013) Geology of Nigeria's sedimentary basins. CSS Bookshop Limited, pp 565

Obahiagbon FI, Oboh H, Uwumarongie-Ilori GE, Agho I (2011) Selenium contents of some commonlyconsumed nigerian vegetables and physiological implications. Chem Soc Nigeria 36(2):2011

Ofoegbu CO (1984) A model for the tectonic evolution of the Benue Trough of Nigeria. Geol Rundsch 73(3):1007–1018. https://doi.org/10.1007/BF01820885

Okoro AU, Igwe EO (2018) Lithostratigraphic characterization of the upper Campanian-Maastrichtian succession in the Afikpo Subbasin, southern Anambra Basin, Nigeria. J Afr Earth Sci 147:178–189. https://doi.org/10.1016/j.jafrearsci.2018.06.021

Olatunde Popoola S, Han XQ, Wang YJ, Qiu ZY, Ye Y (2019) Geochemical investigations of Fe-Si-Mn oxyhydroxides deposits in wocan hydrothermal field on the slow-spreading carlsberg ridge, Indian Ocean: constraints on their types and origin. Minerals 9(1):19. https://doi.org/10.3390/min9010019

Oldfield JE (1999) Selenium World Atlas. Selenium-Tellurium Development Association, Grimberger, Belgium

Poole FG, Desborough GA, Wahlberg JS (1979) Selenium in Paleozoic eugeosynclinal rocks in central Nevada. US Geol Survey Prof Paper 1150:5

Rayman MP (2000) The importance of selenium to human health. The lancet 356(9225):233–241.

Rayman MP (2020) Selenium intake, status, and health: a complex relationship. Hormones 19(1):9–14. https://doi.org/10.1007/s42000-019-00125-5

Reijers TJA, Petters SW, Nwajide CS (1996) The Niger Delta Basin. In: Reijers TJA (ed) Selected Chapters on Geology: SPDC corporate reprographic services. Elsevier, Warri Nigeria, pp 103–114

Sakr TM, Korany M, Katti KV (2018) Selenium nanomaterials in biomedicine: an overview of new opportunities in nanomedicine of selenium. J Drug Deliv Sci Technol 46:223–233. https://doi.org/10.1016/j.jddst.2018.05.023

Salonen J, Alfthan G, Huttunen J, Pikkarainen J, Puska P (1982) Association between cardiovascular death and myocardial infarction and serum selenium in a matched-pair longitudinal study. Lancet 320(8291):175–179. https://doi.org/10.1016/s0140-6736(82)91028-5

Short KC, Stauble AJ (1967) Outline of geology of Niger Delta. AAPG Bull 51:761–779. https://doi.org/10.1306/5d25c0cf-16c1-11d7-8645000102c1865d

Tian H, Ma ZZ, Chen XL, Zhang HY, Bao ZY, Wei CH, Xie SY, Wu ST (2016) Geochemical characteristics of selenium and its correlation to other elements and minerals in selenium-enriched rocks in Ziyang County, Shaanxi Province, China. J Earth Sci 27(5):763–776. https://doi.org/10.1007/s12583-016-0700-x

Tijani MN, Nton ME, Kitagawa R (2010) Textural and geochemical characteristics of the Ajali Sandstone, Anambra Basin, SE Nigeria: implication for its provenance. Comptes Rendus Géoscience 342(2):136–150. https://doi.org/10.1016/j.crte.2009.09.009

Tribovillard N, Algeo TJ, Lyons T Riboulleau A, (2006) Trace metals as paleoredox and paleoproductivityproxies: An update. Che geolo 232(1-2):12-32.

Tribovillard, N, Algeo TJ, Baudin F. Riboulleau AJCG (2012) Analysis of marine environmental conditionsbased onmolybdenum–uranium covariation—Applications to Mesozoic paleoceanography. Che Geolo 324:46–58.

Turgeon S, Brumsack HJ (2006) Anoxic vs dysoxic events reflected in sediment geochemistry during the Cenomanian–Turonian Boundary Event (Cretaceous) in the Umbria–Marche Basin of central Italy. Chem Geol 234(3–4):321–339. https://doi.org/10.1016/j.chemgeo.2006.05.008

Van Ryssen JBJ (2006) An evaluation of the trace element nutritional status of grazers in the eastern regions of the Free State and Mpumalanga. SA-Anim Sci 7:22–30

Wang ZJ, Gao YX (2001) Biogeochemical cycling of selenium in Chinese environments. Appl Geochem 16(11–12):1345–1351. https://doi.org/10.1016/s0883-2927(01)00046-4

Wang M, Li B, Li S, Song Z, Kong F, Zhang X, (2021) Selenium in wheat from farming to food. J Agri and food chem 69(51):15458–15467.

Wedepohl KH (1971) Environmental influences on the chemical composition of shales and clays. Phys Chem Earth 8:307–333. https://doi.org/10.1016/0079-1946(71)90020-6

Wedepohl KH (1991) Chemical composition and fractionation of the continental crust. Geol Rundsch 80(2):207–223. https://doi.org/10.1007/BF01829361

Wijnja H, Schulthess CP (2002) Effect of carbonate on the adsorption of selenate and sulfate on goethite. Soil Sci Soc Am J 66(4):1190–1197. https://doi.org/10.2136/sssaj2002.1190

Winkel LHE, Johnson CA, Lenz M, Grundl T, Leupin OX, Amini M, Charlet L (2012) Environmental selenium research: from microscopic processes to global understanding. Environ Sci Technol 46(2):571–579. https://doi.org/10.1021/es203434d

Xu ZN, Lin ZQ, Zhao GS, Guo YB (2024) Biogeochemical behavior of selenium in soil-air-water environment and its effects on human health. Int J Environ Sci Technol 21(1):1159–1180. https://doi.org/10.1007/s13762-023-05169-0

Yakubu D, Dawet A, Olaleye NA (2014) Effects of vitamin E and selenium on some blood parameters of trypanosoma brucei brucei infected rats. Br J Appl Sci Technol 4(7):1100–1108. https://doi.org/10.9734/bjast/2014/5732

Zaborski PMP (1983) (1983) Campano-maastrichtian ammonites, correlation and palaeogeography in Nigeria. J Afr Earth Sci 1(1):59–63. https://doi.org/10.1016/0899-5362(83)90032-5

Zhang BY, Cheng W, Zhang Q, Li YJ, Sun PC, Fathy D (2022) Occurrence patterns and enrichment influencing factors of trace elements in Paleogene coal in the Fushun Basin, China. ACS Earth Space Chem 6(12):3031–3042. https://doi.org/10.1021/acsearthspacechem.2c00263

Zheng YH, Xie T, Li SL, Wang W, Wang YJ, Cao ZJ, Yang HJ (2022) Effects of selenium as a dietary source on performance, inflammation, cell damage, and reproduction of livestock induced by heat stress: a review. Front Immunol 12:820853. https://doi.org/10.3389/fimmu.2021.820853

Zhou CQ, Huang JC, Liu F, He SB, Zhou WL (2019) Selenium removal and biotransformation in a floating-leaved macrophyte system. Environ Pollut 245:941–949. https://doi.org/10.1016/j.envpol.2018.11.096